

STOLAS: STOchastic LAttice Simulation of cosmic inflation



Yurino Mizuguchi,^a Tomoaki Murata,^b and Yuichiro Tada^{c,a}

^aDepartment of Physics, Nagoya University,
Furo-cho Chikusa-ku, Nagoya 464-8602, Japan

^bDepartment of Physics, Rikkyo University,
Toshima, Tokyo 171-8501, Japan

^cInstitute for Advanced Research, Nagoya University,
Furo-cho Chikusa-ku, Nagoya 464-8601, Japan

E-mail: mizuguchi.yurino.y0@s.mail.nagoya-u.ac.jp, tmurata@rikkyo.ac.jp,
tada.yuichiro.y8@f.mail.nagoya-u.ac.jp

Abstract. We develop a C++ package of the STOchastic LAttice Simulation (STOLAS) of cosmic inflation. It performs the numerical lattice simulation in the application of the stochastic- δN formalism. STOLAS can directly compute the three-dimensional map of the observable curvature perturbation without estimating its statistical properties. In its application to two toy models of inflation, chaotic inflation and Starobinsky's linear-potential inflation, we confirm that STOLAS is well-consistent with the standard perturbation theory. Furthermore, by introducing the importance sampling technique, we have success in numerically sampling the current abundance of primordial black holes (PBHs) in a non-perturbative way. The package is available [here](#).

ArXiv ePrint: [2405.10692](https://arxiv.org/abs/2405.10692)

Contents

1	Introduction	1
2	STOchastic LAttice Simulation	2
2.1	Stochastic formalism of inflation	3
2.2	Discretisation	6
2.3	Stochastic- $\delta\mathcal{N}$	9
3	Primary statistics	11
3.1	Calculation of power spectrum	11
3.2	Chaotic inflation	11
3.3	Starobinsky's linear potential	13
4	Importance sampling for primordial black holes	15
4.1	Review of PBH formation	15
4.2	Importance sampling	18
4.3	Results and Discussion	20
5	Conclusions	24
A	Derivation of the power spectrum of the scalar field at NLO in slow-roll	25

1 Introduction

Cosmic inflation, the accelerated expansion phase of the early universe, is a widely accepted scenario of the dawn of our universe. Not only does it realise a globally flat and homogeneous universe, but inflation can also provide local fluctuations in the metric or the energy density by stretching the quantum vacuum fluctuation, those primordial perturbations growing into the current rich structures of the universe such as galaxies and clusters. Since its advent [1–6], a tremendous number of inflation models have been proposed, but its concrete mechanism is yet to be clarified despite the significant improvement in its understanding through the cosmological observations represented by the Planck measurements [7] of the cosmic microwave background (CMB) anisotropies. To figure out its whole aspect, further detailed studies on the properties of the generated primordial perturbation as well as the deep observations of cosmological structures as its descendants are necessary.

Speaking of the connection between the primordial perturbation and the late-time observables, the importance of numerical simulations such as N -body simulations for dark matter halos and hydrodynamic simulations for galaxy formations (see, e.g., Ref. [8] for a recent review on cosmological simulations) has been increasing more and more. The lattice simulation of inflation [9–14] has started to attract attention but has been less developed compared to the simulations of the late universe. One of the potential issues in the development of simulations of inflation is that quantum mechanics and the theory of gravity, the two principal elements of inflation, are unified only in a perturbative manner and no guidance principle for a non-perturbative simulation has been clarified yet.

The *stochastic formalism* of inflation (see Refs. [15–24] for the first works and Ref. [25] for a recent review) can bring about a breakthrough in this situation. It is an effective theory for superHubble coarse-grained fields (IR modes) which is obtained by integrating out the other UV modes perturbatively (and hence the quantum theory of gravity is well-defined at least at tree level). The IR modes are well approximated by classical fields and the horizon exit of the UV modes are treated as classical stochastic noise onto the IR modes. Furthermore, the gradient expansion (the long-wavelength approximation) justifies, at its lowest order, the assumption that the IR spacetime locally reads the flat Friedmann–Lemaître–Robertson–Walker (FLRW) universe, which significantly simplifies the computation. In this way, the stochastic formalism can provide a guidance principle for a numerical lattice simulation of the superHubble IR fields. Coarse-graining in this formalism has a good compatibility with a lattice simulation as it anyway needs to “discretise” the spacetime.

The lattice simulation of stochastic inflation has been done by Salopek and Bond [26] for the first time to simulate the inflaton field’s fluctuation, but not for the observable curvature perturbation. To calculate the curvature perturbation in the stochastic formalism, the *stochastic- δN* technique has been intentionally developed in recent years (see Refs. [27–29] for the first papers and also Refs. [30–32] for applications to numerical simulations other than lattice). In this work, we propose a C++ package, STOCHASTIC LATTICE SIMULATION (STOLAS), for the curvature perturbation in combination with the stochastic- δN formalism and the numerical lattice simulation.

The paper is organised as follows. In Sec. 2, we review the stochastic formalism and provide the implementation of STOLAS. In Sec. 3, we show that STOLAS successfully reproduce the primary statistics such as the power spectrum and the non-linearity parameter of the curvature perturbation. In Sec. 4, we exemplify the calculation of the primordial black hole (PBH) mass function as a powerful application of STOLAS. PBHs are the productions of $\mathcal{O}(1)$ fluctuations which are good targets of the non-perturbative simulation. Also, it has been recently claimed that the PBH formation criterion is sensitive to the spatial profile of the large perturbation (see, e.g., Refs. [33, 34]), which can be simulated by the position-space lattice computation. The *importance sampling* technique (see Ref. [35] in the context of stochastic inflation) enables us to sample the PBH formation, the statistically rare event. Sec. 5 is devoted to conclusions. We adopt the natural unit $c = \hbar = 1$ throughout the paper.

2 STOchastic LAttice Simulation

Our STOLAS implements the stochastic formalism of inflation in the numerical lattice simulation. Though the basic idea has already been proposed in 1991 by Salopek and Bond [26], it has long been out of the spotlight. The significant development in computational resources provides more opportunities for numerical simulations than in those days. Furthermore, the recent stochastic- δN technique [27–29] enables us to calculate not only the inflatons’ fluctuations but also the observable curvature perturbations. In this section, we first review the stochastic formalism of inflation and then describe its implementation in the discrete lattice simulation.

2.1 Stochastic formalism of inflation

Let us review the stochastic formalism of inflation in this subsection. First, we start from the action of general relativity and a canonical scalar field ϕ :¹

$$S = \int d^4x \sqrt{-g} \left[\frac{1}{2} M_{\text{Pl}}^2 R - \frac{1}{2} g^{\mu\nu} \partial_\mu \phi \partial_\nu \phi - V(\phi) \right]. \quad (2.1)$$

R is the Ricci scalar associated with the spacetime metric $g_{\mu\nu}$, $V(\phi)$ is the scalar potential, and $M_{\text{Pl}} = 1/\sqrt{8\pi G}$ is the reduced Planck mass. We adopt the Arnowitt–Deser–Misner (ADM) decomposition of the spacetime metric as

$$ds^2 = -\mathcal{N}^2 dt^2 + \gamma_{ij} (dx^i + \beta^i dt)(dx^j + \beta^j dt), \quad (2.2)$$

where \mathcal{N} is the lapse function, β^i is the shift vector, and γ_{ij} is the spatial metric. The corresponding Lagrangian density $S = \int dt d^3x \mathcal{L}$ reads

$$\mathcal{L} = \mathcal{N} \sqrt{\gamma} \left[\frac{M_{\text{Pl}}^2}{2} (R^{(3)} + K_{ij} K^{ij} - K^2) + \frac{1}{2\mathcal{N}^2} v^2 - \frac{1}{2} \gamma^{ij} \partial_i \phi \partial_j \phi - V(\phi) \right]. \quad (2.3)$$

Here, $\gamma = \det \gamma_{ij}$, $R^{(3)}$ is the corresponding spatial Ricci curvature,

$$K_{ij} = \frac{1}{2\mathcal{N}} (2\beta_{(i|j)} - \dot{\gamma}_{ij}), \quad (2.4)$$

is the extrinsic curvature (where dots denote time derivatives, the symbol $|$ indicates the covariant derivative associated with γ_{ij} , and the parentheses signal symmetrisation), $K = K_i^i$ is its trace where the spacial indices are raised and lowered by γ_{ij} and its inverse γ^{ij} , and

$$v = \dot{\phi} - \beta^i \partial_i \phi. \quad (2.5)$$

This Lagrangian is followed by the constraint equations

$$C = C_i = 0, \quad (2.6)$$

with

$$\begin{aligned} C &= \frac{2}{\gamma M_{\text{Pl}}^2} \left[\pi_{ij} \pi^{ij} - \frac{1}{2} (\pi_i^i)^2 \right] - \frac{M_{\text{Pl}}^2}{2} R^{(3)} + \frac{1}{2\gamma} \pi_{\text{I}}^2 + \frac{\gamma^{ij}}{2} \partial_i \phi \partial_j \phi + V, \\ C_i &= -2 \left(\frac{\pi_i^j}{\sqrt{\gamma}} \right)_{|j} + \frac{1}{\sqrt{\gamma}} \pi_{\text{I}} \partial_i \phi = \frac{1}{\sqrt{\gamma}} \left(-2\partial_k (\gamma_{ij} \pi^{jk}) + \pi^{jk} \partial_i \gamma_{jk} + \pi_{\text{I}} \partial_i \phi \right), \end{aligned} \quad (2.7)$$

and equations of motion (EoMs) (in the scalar sector)

$$\begin{aligned} \dot{\phi} &= \frac{\mathcal{N}}{\sqrt{\gamma}} \pi_{\text{I}} + \beta^i \partial_i \phi, \\ \dot{\pi}_{\text{I}} &= -\sqrt{\gamma} \mathcal{N} V' + \partial_i (\sqrt{\gamma} \mathcal{N} \gamma^{ij} \partial_j \phi) + \partial_i (\beta^i \pi_{\text{I}}), \end{aligned} \quad (2.8)$$

with the conjugate momenta (the subscript “I” stands for “inflaton”)

$$\pi_{\text{I}} = \frac{\partial \mathcal{L}}{\partial \dot{\phi}} = \frac{\sqrt{\gamma}}{\mathcal{N}} v, \quad \pi^{ij} = \frac{\partial \mathcal{L}}{\partial \dot{\gamma}_{ij}} = \frac{M_{\text{Pl}}^2}{2} \sqrt{\gamma} (K \gamma^{ij} - K^{ij}). \quad (2.9)$$

¹See, e.g., Ref. [36] for a generalisation to multiple scalar fields.

For convenience (and conceptual relevance; see, e.g., Ref. [37]), we employ the e-folding number N as the time variable and take the spatially flat gauge, neglecting the vector and tensor perturbations:

$$\gamma_{ij}(N, \mathbf{x}) = a^2(N)\delta_{ij}, \quad a(N) \propto e^N, \quad (2.10)$$

where the scale factor $a(N)$ is spatially homogeneous. Relevant equations are simplified in this gauge as $R^{(3)}$ vanishes and $\sqrt{\gamma} = a^3$. Hereafter, we also rescale the inflaton momentum as $\pi_{\mathbf{I}} \rightarrow a^3\pi_{\mathbf{I}}$.

In stochastic inflation, the physical variables (represented by the symbol X) are decomposed into the superHubble “IR” part and the other “UV” part as

$$\begin{aligned} X_{\text{IR}}(N, \mathbf{x}) &= \int \frac{d^3k}{(2\pi)^3} e^{i\mathbf{k}\cdot\mathbf{x}} X_{\mathbf{k}}(N) \Theta(\sigma a(N)\mathbf{H} - k), \\ X_{\text{UV}}(N, \mathbf{x}) &= X(N, \mathbf{x}) - X_{\text{IR}}(N, \mathbf{x}), \end{aligned} \quad (2.11)$$

where $\Theta(z)$ is the Heaviside step function,²

$$\Theta(z) = \begin{cases} 0 & \text{for } z < 0, \\ 1 & \text{for } z > 0. \end{cases} \quad (2.12)$$

The dimensionless and dimensionful parameters σ and \mathbf{H} are chosen so that $k_\sigma := \sigma a(N)\mathbf{H} \ll a(N)H(N, \mathbf{x})$ for relevant spacetime points and realisations, where the local Hubble parameter $H(N, \mathbf{x})$ is defined below.³ Practically, we will fix \mathbf{H} by the global Hubble parameter at the simulation starting time and σ by a positive and small number, $\sigma \ll 1$.

We characterise the decomposed variables in our setup as

$$\begin{aligned} \phi &= \varphi + Q, & \pi_{\mathbf{I}} &= \varpi + P, \\ \mathcal{N} &= \mathcal{N}_{\text{IR}} + \alpha, & \beta^i &= a^{-2}\delta^{ij}\partial_j\psi. \end{aligned} \quad (2.13)$$

φ , ϖ , and \mathcal{N}_{IR} are IR while Q , P , α , and ψ are UV. We fixed $\beta_{\text{IR}}^i = 0$ as it is a pure gauge choice in the long-wavelength limit.⁴ Substituting them into the constraints (2.6) and EoMs (2.8), keeping terms at all orders in IR but up to linear order in UV, and dropping the spatial derivatives of IR quantities, one finds

$$\begin{aligned} \frac{d\varphi(N, \mathbf{x})}{dN} &= \frac{\varpi(N, \mathbf{x})}{H(N, \mathbf{x})} + \xi_\phi(N, \mathbf{x}), \\ \frac{d\varpi(N, \mathbf{x})}{dN} &= -3\varpi(N, \mathbf{x}) - \frac{V'(\varphi(N, \mathbf{x}))}{H(N, \mathbf{x})} + \xi_\pi(N, \mathbf{x}), \end{aligned} \quad (2.14)$$

²The consistent definition of $\Theta(z)$ at $z = 0$ requires a detailed discussion of the discretisation of the path integral. See Refs. [38, 39].

³The literature often chooses $\sigma a(N)H(N, \mathbf{x})$ with a positive small parameter $\sigma \ll 1$ as the IR cutoff scale. Though the Hubble parameter is practically almost constant, this cutoff is spatial-dependent and circularly defined as the local Hubble parameter itself is defined by the IR quantities, strictly speaking. Hence, the consistent definition of the stochastic formalism in this way is tough and non-trivial. Our choice of the cutoff seems less physical but can avoid all these problems. From the viewpoint of the lattice simulation, \mathbf{H} can be understood as a parameter of the grid size and causes no problem as long as $\sigma a(N)\mathbf{H} \ll a(N)H(N, \mathbf{x})$.

⁴The long-wavelength shift may be non-local and affect the formulation of the stochastic equation for the non-attractor models. See, e.g., Ref. [40] for the details.

for the IR part and the linearised equations

$$\begin{aligned}\frac{dQ_{\mathbf{k}}}{dN} &= \frac{P_{\mathbf{k}}}{H} + \frac{\varpi^2}{2M_{\text{Pl}}^2 H^2} Q_{\mathbf{k}}, \\ \frac{dP_{\mathbf{k}}}{dN} &= -3P_{\mathbf{k}} - \frac{k^2}{a^2 H} Q_{\mathbf{k}} - \frac{1}{H} \left(V'' + \frac{V' \varpi}{M_{\text{Pl}}^2 H} + \frac{3\varpi^2}{2M_{\text{Pl}}^2} \right) Q_{\mathbf{k}} - \frac{\varpi^2}{2M_{\text{Pl}}^2 H^2} P_{\mathbf{k}},\end{aligned}\tag{2.15}$$

for the UV part, which can be summarised into the standard Mukhanov–Sasaki equation (A.3) (see, e.g., Ref. [36]). The local Hubble parameter is defined by $H = 1/\mathcal{N}_{\text{IR}}$ and calculated via the local Friedmann equation

$$\frac{3M_{\text{Pl}}^2}{\mathcal{N}_{\text{IR}}^2(N, \mathbf{x})} = 3M_{\text{Pl}}^2 H^2(N, \mathbf{x}) = \frac{\varpi^2(N, \mathbf{x})}{2} + V(\varphi(N, \mathbf{x})),\tag{2.16}$$

derived from the constraint equation (2.6).

ξ 's in the IR EoM (2.14) are defined by

$$\begin{aligned}\xi_{\phi}(N, \mathbf{x}) &= \int \frac{d^3 k}{(2\pi)^3} e^{i\mathbf{k}\cdot\mathbf{x}} Q_{\mathbf{k}}(N) \partial_N \Theta(\sigma a(N)H - k), \\ \xi_{\pi}(N, \mathbf{x}) &= \int \frac{d^3 k}{(2\pi)^3} e^{i\mathbf{k}\cdot\mathbf{x}} P_{\mathbf{k}}(N) \partial_N \Theta(\sigma a(N)H - k),\end{aligned}\tag{2.17}$$

as a consequence of the time-dependent cutoff $\sigma a(N)H$. Physically, they represent the horizon exit of subHubble modes. While the UV mode is understood as a quantum vacuum fluctuation, the superHubble IR mode is well approximated as a classical field. The ξ terms hence have an intermediate feature: classical but random variables originating from the quantum vacuum fluctuation. Their statistical nature should be determined by the quantum theoretical expectation as (see, e.g., Ref. [24] for the detailed derivation)⁵

$$\langle \xi_X \rangle = 0, \quad \langle \xi_X(N, \mathbf{x}) \xi_Y(N', \mathbf{x}') \rangle = \mathcal{P}_{XY}(N, k_{\sigma}(N)) \frac{\sin k_{\sigma} r}{k_{\sigma} r} \delta(N - N'),\tag{2.18}$$

where X and Y represent ϕ or π , $r = |\mathbf{x} - \mathbf{x}'|$ is the distance between \mathbf{x} and \mathbf{x}' , and the dimensionless power spectrum $\mathcal{P}_{XY}(N, k)$ is defined by

$$\langle Q_{X, \mathbf{k}}(N) Q_{Y, \mathbf{k}'}(N) \rangle = (2\pi)^3 \delta^{(3)}(\mathbf{k} + \mathbf{k}') \frac{2\pi^2}{k^3} \mathcal{P}_{XY}(N, k),\tag{2.19}$$

in the notation $Q_{\phi, \mathbf{k}}(N) = Q_{\mathbf{k}}(N)$ and $Q_{\pi, \mathbf{k}}(N) = P_{\mathbf{k}}(N)$. The bracket in Eq. (2.19) denote the quantum average, while other brackets in Eq. (2.18) and hereafter stand for the stochastic average. Practically, the momentum noise is suppressed as $\mathcal{P}_{\phi\pi} \sim \mathcal{O}(\sigma^2)$ and $\mathcal{P}_{\pi\pi} \sim \mathcal{O}(\sigma^4)$

⁵ ξ_{ϕ} and ξ_{π} should be real because φ and ϖ are. However, the cross power spectrum $\mathcal{P}_{\phi\pi}$ is not necessarily real in the definition (2.19). It exhibits the limitation of the “heuristic” derivation of the stochastic formalism here. In a more sophisticated path-integral approach, one finds $\langle \xi_{\phi} \xi_{\pi} \rangle = \langle \xi_{\pi} \xi_{\phi} \rangle \propto \text{Re} \mathcal{P}_{\phi\pi}$; see Ref. [36]. In this paper, we merely neglect ξ_{π} hereafter and hence this subtlety is not problematic.

in a single-field slow-roll model.⁶ We hence neglect ξ_π and adopt the approximated EoM,

$$\begin{aligned}\frac{d\varphi(N, \mathbf{x})}{dN} &\simeq \frac{\varpi(N, \mathbf{x})}{H(N, \mathbf{x})} + \mathcal{P}_\phi^{1/2}(N, k_\sigma(N))\xi(N, \mathbf{x}), \\ \frac{d\varpi(N, \mathbf{x})}{dN} &\simeq -3\varpi(N, \mathbf{x}) - \frac{V'(\varphi(N, \mathbf{x}))}{H(N, \mathbf{x})},\end{aligned}\tag{2.20}$$

with the renormalised noise,

$$\langle \xi \rangle = 0, \quad \langle \xi(N, \mathbf{x})\xi(N', \mathbf{x}') \rangle = \frac{\sin k_\sigma r}{k_\sigma r} \delta(N - N').\tag{2.21}$$

2.2 Discretisation

In the numerical lattice simulation, we solve the dynamics of the stochastic inflation in the discretised spacetime with the time step ΔN and the grid size Δx within the comoving box L on a side. $N_L = \frac{L}{\Delta x} + 1$ is the number of grids per side. We will take $N_L = 64$ and our formulation will be based on the assumption that N_L is an even number (a power of two, more specifically, to utilise the fast Fourier transformation algorithm).

In the simplest Euler–Maruyama method (but the application to a higher-order method is straightforward; see, e.g., Ref. [45]), the EoM (2.20) is discretised as⁷

$$\begin{aligned}\varphi(N + \Delta N, \mathbf{x}) - \varphi(N, \mathbf{x}) &= \Delta\varphi_D(N, \mathbf{x}) + \mathcal{P}_\phi^{1/2}(N, k_\sigma(N))\Delta W(N, \mathbf{x}), \\ \varpi(N + \Delta N, \mathbf{x}) - \varpi(N, \mathbf{x}) &= \Delta\varpi_D(N, \mathbf{x})\end{aligned}\tag{2.22}$$

with the differences in the deterministic part

$$\Delta\varphi_D(N, \mathbf{x}) = \frac{\varpi(N, \mathbf{x})}{H(N, \mathbf{x})}\Delta N, \quad \Delta\varpi_D(N, \mathbf{x}) = \left(-3\varpi(N, \mathbf{x}) - \frac{V'(\varphi(N, \mathbf{x}))}{H(N, \mathbf{x})}\right)\Delta N,\tag{2.23}$$

and the Gaussian random variable ΔW satisfying

$$\langle \Delta W \rangle = 0, \quad \langle \Delta W(N, \mathbf{x})\Delta W(N', \mathbf{x}') \rangle = \frac{\sin k_\sigma r}{k_\sigma r} \delta_{NN'} \Delta N.\tag{2.24}$$

For stability, we adopt the fourth-order Runge–Kutta (RK4) method to evaluate the deterministic part $\Delta\varphi_D$ and $\Delta\varpi_D$.

The spatial dependence (2.24) can be realised with the use of the discrete Fourier space. We define the discrete Fourier and inverse Fourier transformation by

$$\Delta W_{\mathbf{n}}(N) = \sum_{\mathbf{x}} \Delta W(N, \mathbf{x}) e^{-i\frac{2\pi}{L}\mathbf{n}\cdot\mathbf{x}}, \quad \Delta W(N, \mathbf{x}) = \frac{1}{N_L^3} \sum_{\mathbf{n}} \Delta W_{\mathbf{n}}(N) e^{i\frac{2\pi}{L}\mathbf{n}\cdot\mathbf{x}},\tag{2.25}$$

⁶Beyond this assumption such as the ultra-slow-roll (USR) models, the momentum noise can be non-negligible (see, e.g., Refs. [41–43]), though its implementation in STOLAS is straightforward. We have confirmed that the power spectra in our two examples in Secs. 3 and 4 are well consistent with the prediction of the Mukhanov–Sasaki equation even without the momentum noise, particularly around the peak of the power spectrum in Starobinsky’s linear-potential model. The momentum noise could be relevant around the dip of the power spectrum in the USR models [44].

⁷Note that the stochastic differential equation should be discretised in Itô’s way in the stochastic inflation (see Refs. [38, 39]). The noise coefficient \mathcal{P}_ϕ is hence evaluated at the time N for the increment at N . Itô’s discretisation generally breaks the field-space covariance [46]. Hence, in the curved-field-space multi-field models, the derivative should be replaced by the Itô covariant derivative to keep the field-space covariance. See Ref. [36] for the details.

where $\mathbf{n} = (n_x, n_y, n_z)$, ($n_i \in \{0, 1, 2, \dots, N_L - 1\}$) is the wave vector. Note that the discrete Fourier mode exhibits the following periodicity:

$$\Delta W_{(n_x, n_y, n_z)} = \Delta W_{(n_x + L, n_y, n_z)} = \Delta W_{(n_x, n_y + L, n_z)} = \Delta W_{(n_x, n_y, n_z + L)}. \quad (2.26)$$

It enables us to shift the wave vector domain to $\tilde{\mathbf{n}} = (\tilde{n}_x, \tilde{n}_y, \tilde{n}_z)$, ($\tilde{n}_i \in \{-\frac{N_L}{2} + 1, -\frac{N_L}{2} + 2, \dots, \frac{N_L}{2}\}$) with the definition

$$\tilde{n}_i = \begin{cases} n_i & \text{for } n_i \leq N_L/2, \\ n_i - N_L & \text{otherwise,} \end{cases} \Leftrightarrow n_i = \begin{cases} \tilde{n}_i & \text{for } \tilde{n}_i \geq 0, \\ \tilde{n}_i + N_L & \text{for otherwise.} \end{cases} \quad (2.27)$$

The original indexation is conventional for the fast Fourier transformation, while the reality condition in Fourier space,

$$\Delta W_{\mathbf{n}} = \Delta W_{-\mathbf{n}}^* \quad (2.28)$$

is easy to handle in the shifted one.

Due to the reality condition, only the half of $\Delta W_{\mathbf{n}}$ is independent. We specify the set \mathcal{C} of the independent points by

$$\mathcal{C} = \bigcup_{i=1}^5 \mathcal{C}_i, \quad (2.29)$$

where

$$\begin{aligned} \mathcal{C}_1 &= \left\{ \mathbf{n} \left| 1 \leq \tilde{n}_x \leq \frac{N_L}{2} - 1, \tilde{n}_y \neq \frac{N_L}{2}, \tilde{n}_z \neq \frac{N_L}{2} \right. \right\}, \\ \mathcal{C}_2 &= \left\{ \mathbf{n} \left| \tilde{n}_x = \frac{N_L}{2}, \tilde{n}_y \neq \frac{N_L}{2}, 1 \leq \tilde{n}_z \leq \frac{N_L}{2} - 1 \right. \right\} \cup (2 \text{ even perms.}), \\ \mathcal{C}_3 &= \left\{ \mathbf{n} \left| \tilde{n}_x = 0, \tilde{n}_y \neq \frac{N_L}{2}, 1 \leq \tilde{n}_z \leq \frac{N_L}{2} - 1 \right. \right\}, \\ \mathcal{C}_4 &= \left\{ \mathbf{n} \left| \tilde{n}_x = \tilde{n}_y = \frac{N_L}{2}, 1 \leq \tilde{n}_z \leq \frac{N_L}{2} - 1 \right. \right\} \cup (2 \text{ perms.}), \\ \mathcal{C}_5 &= \left\{ \mathbf{n} \left| \tilde{n}_x = \tilde{n}_z = 0, 1 \leq \tilde{n}_y \leq \frac{N_L}{2} - 1 \right. \right\} \\ &\quad \cup \left[\left\{ \mathbf{n} \left| \tilde{n}_x = \frac{N_L}{2}, 1 \leq \tilde{n}_y \leq \frac{N_L}{2} - 1, \tilde{n}_z = 0 \right. \right\} \cup (2 \text{ even perms.}) \right]. \end{aligned} \quad (2.30)$$

Each set \mathcal{C}_i includes the points of $(N_L/2-1)(N_L-1)^2$, $3(N_L/2-1)(N_L-1)$, $(N_L/2-1)(N_L-1)$, $3(N_L/2-1)$, and $4(N_L/2-1)$, reaching $(N_L^3-8)/2$ points in total. As they are complex, they correspond to (N_L^3-8) real degrees of freedom (DoFs). The remaining eight DoFs correspond to the following eight points:

$$\mathcal{R} = \left\{ \mathbf{n} \left| \tilde{n}_i = 0 \text{ or } \frac{N_L}{2} \quad (i = x, y, z) \right. \right\}. \quad (2.31)$$

Their reflecting points are congruent to the original points modulo N_L :

$$\tilde{\mathbf{n}} - (-\tilde{\mathbf{n}}) = 2\tilde{\mathbf{n}} = (nN_L, mN_L, kN_L), \quad n, m, k \in \mathbb{Z}, \quad \text{for } \tilde{\mathbf{n}} \in \mathcal{R}. \quad (2.32)$$

It hence follows from the periodicity (2.26) and the reality condition (2.28) that $\Delta W_{\mathbf{n}}$ for $\mathbf{n} \in \mathcal{R}$ is real. The N_L^3 real DoFs expected in the position space are exhausted in total.

Finally, the spatial correlation (2.24) can be realised if $\Delta W_{\mathbf{n}}$ is non-zero only for $2\pi\tilde{n}/L = k_\sigma$. Practically, we allow a small error for this condition, taking account of the discreteness of \tilde{n} itself, as

$$\varsigma(N) = \left\{ \mathbf{n} \left| |\tilde{n} - n_\sigma(N)| \leq \frac{\Delta n_\sigma}{2} \right. \right\}, \quad n_\sigma(N) = \frac{k_\sigma(N)L}{2\pi}, \quad (2.33)$$

where we choose $\Delta n_\sigma = 1$. The noise distribution is then determined at each time step by

$$\begin{cases} \text{Re}[\Delta W_{\mathbf{n}}(N)] \sim \text{Im}[\Delta W_{\mathbf{n}}(N)] \sim \mathfrak{N}\left(0, \frac{N_L^6}{2|\varsigma(N)|} \Delta N\right) & \text{for } \mathbf{n} \in \mathcal{C} \cap \varsigma(N), \\ \Delta W_{\mathbf{n}}(N) \sim \mathfrak{N}\left(0, \frac{N_L^6}{|\varsigma(N)|} \Delta N\right) & \text{for } \mathbf{n} \in \mathcal{R} \cap \varsigma(N), \\ \Delta W_{\mathbf{n}}(N) = \Delta W_{\bar{\mathbf{n}}}^* & \text{for } \mathbf{n} \in \overline{(\mathcal{C} \cup \mathcal{R})} \cap \varsigma(N), \\ \Delta W_{\mathbf{n}}(N) = 0 & \text{otherwise,} \end{cases} \quad (2.34)$$

where $\mathfrak{N}(\mu, \sigma^2)$ is the normal distribution with the mean μ and the variance σ^2 . Here, the symbol “ \sim ” means that the random variables on both sides follow the same probability distribution, while the equal sign “ $=$ ” is used only if they take the same values. $|\varsigma(N)|$ is the number of elements of $\varsigma(N)$, and $\bar{\mathbf{n}}$ is the grid point congruent to $-\mathbf{n}$ modulo N_L :

$$\bar{n}_i = \begin{cases} 0 & \text{for } n_i = 0, \\ N_L - n_i & \text{otherwise.} \end{cases} \quad (2.35)$$

With this noise distribution, the spatial correlation is reproduced as

$$\begin{aligned} \langle \Delta W(N, \mathbf{x}) \Delta W(N', \mathbf{x}') \rangle &= \frac{\delta_{NN'}}{N_L^6} \sum_{\mathbf{n}, \mathbf{m}} \langle \Delta W_{\mathbf{n}}(N) \Delta W_{\mathbf{m}}(N) \rangle e^{i\frac{2\pi}{L}(\mathbf{n}\cdot\mathbf{x} + \mathbf{m}\cdot\mathbf{x}')} \\ &= \frac{\delta_{NN'} \Delta N}{|\varsigma(N)|} \left[\sum_{\substack{\mathbf{n} \in \mathcal{C} \cap \varsigma(N), \\ \mathbf{n} \in \overline{(\mathcal{C} \cup \mathcal{R})} \cap \varsigma(N)}} e^{i\frac{2\pi}{L}(\mathbf{n}\cdot\mathbf{x} + \bar{\mathbf{n}}\cdot\mathbf{x}')} + \sum_{\mathbf{n} \in \mathcal{R} \cap \varsigma(N)} e^{i\frac{2\pi}{L}\mathbf{n}\cdot(\mathbf{x} + \mathbf{x}')} \right] \\ &= \frac{\delta_{NN'} \Delta N}{|\varsigma(N)|} \sum_{\mathbf{n} \in \varsigma(N)} e^{i\frac{2\pi}{L}\mathbf{n}\cdot(\mathbf{x} - \mathbf{x}')} \\ &\rightarrow \frac{\delta_{NN'} \Delta N}{4\pi} \int d\Omega e^{i\mathbf{k}_\sigma(N)\cdot(\mathbf{x} - \mathbf{x}')} = \frac{\sin k_\sigma(N)r}{k_\sigma(N)r} \delta_{NN'} \Delta N. \end{aligned} \quad (2.36)$$

Note that $\exp[i\frac{2\pi}{L}\bar{\mathbf{n}}\cdot\mathbf{x}'] = \exp[-i\frac{2\pi}{L}\mathbf{n}\cdot\mathbf{x}']$ for $\mathbf{n} \in \mathcal{C}$ and $\exp[i\frac{2\pi}{L}\mathbf{n}\cdot\mathbf{x}'] = \exp[-i\frac{2\pi}{L}\mathbf{n}\cdot\mathbf{x}']$ for $\mathbf{n} \in \mathcal{R}$. We also used the continuous limit in the last line.

In Fig. 1, we showed samples of the $\Delta W(N, \mathbf{x})$ map at $N = 3.0, 4.0$, and 4.6 corresponding to $n_\sigma \simeq 2.0, 5.5$, and 10 for $\sigma = 0.1$ and the scale factor normalisation $a(N=0)\mathbf{H}L = 2\pi$ at the beginning of the simulation $N = 0$. The correlation $\langle \Delta W(N, \mathbf{x}) \Delta W(N, \mathbf{x}') \rangle$ calculated for these maps as a function of the (normalised) distance $\hat{r} = \frac{N_L}{L} |\mathbf{x} - \mathbf{x}'|$ is also compared with the theoretical requirement $\text{sinc}(k_\sigma r) = \text{sinc}\left(\frac{2\pi n_\sigma}{N_L} \hat{r}\right)$ where $\text{sinc } x = \frac{\sin x}{x}$ is the sine cardinal function. Though the small n_σ map fails due to the discreteness of the lattice, the maps for large enough n_σ successfully reproduce the required correlation.

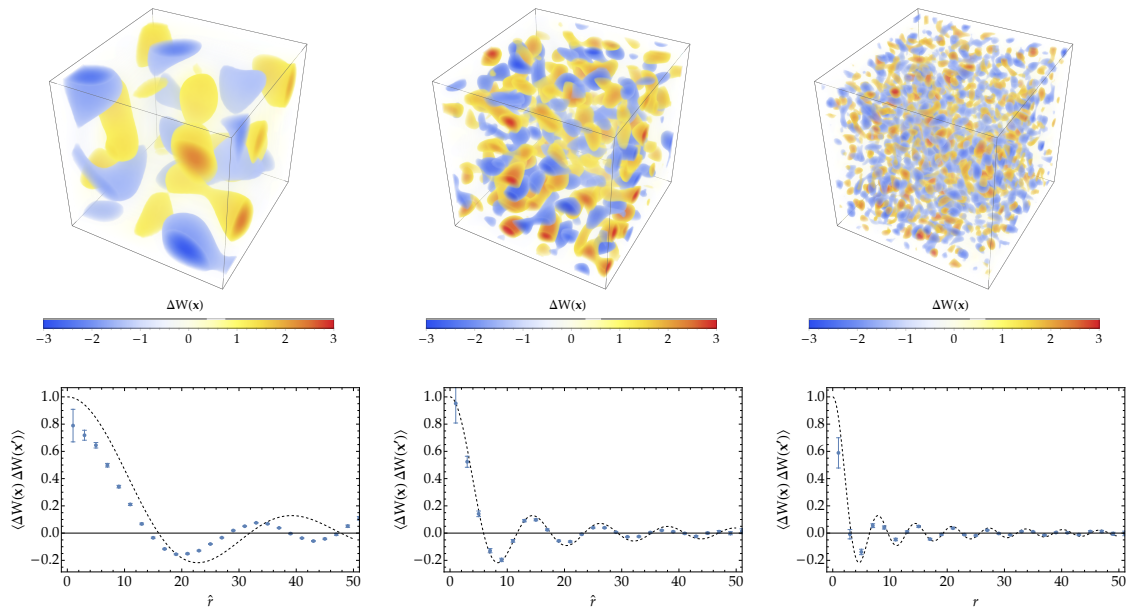


Figure 1. 3D plots of the sample of $\Delta W(N, \mathbf{x})$ (top) and the corresponding spatial correlation $\langle \Delta W(\mathbf{x}) \Delta W(\mathbf{x}') \rangle$ as a function of $\hat{r} = \frac{N_L}{L} |\mathbf{x} - \mathbf{x}'|$ (bottom) at $N = 3.0, 4.0$, and 4.6 corresponding to $n_\sigma \simeq 2.0, 5.5$, and 10 from left to right. In the bottom panels, the blue dots with error bars represent the numerical results, while the black dashed lines are the theoretical requirement $\text{sinc}\left(\frac{2\pi n_\sigma}{N_L} \hat{r}\right)$. The numerical correlation is estimated in the Monte Carlo way, that is, 10^6 pairs of points $(\mathbf{x}, \mathbf{x}')$ are randomly chosen, sorted to the \hat{r} -bin with the width $\Delta \hat{r} = 2$, and the average and the standard error are evaluated for each bin. One finds that the realised noise reproduces the theoretical correlation well for large enough n_σ , while it fails for small n_σ due to the discreteness of the lattice.

We also note that, thanks to our choice of the coarse-graining scale in Eq. (2.11), the noise correlation (2.24) and hence the noise distribution (2.34) are independent of the dynamics and determined only by the time coordinate N . Therefore, we can prepare the noise map data in advance of the simulation.

2.3 Stochastic- $\delta\mathcal{N}$

We have all the ingredients to calculate the inflaton fluctuations (and their conjugate momenta) in the stochastic formalism. However, the inflatons' fluctuations in themselves are not direct observables in the late universe as they decay into daughter particles and disappear after the end of inflation. That is why cosmologists often calculate the conserved quantity on a superHubble scale: the curvature perturbation ζ . Thanks to the $\delta\mathcal{N}$ formalism [47–53], the curvature perturbation (on a uniform-density slice) ζ can be obtained as a fluctuation in the e-folding number, $\delta\mathcal{N}$, between an initial flat-slicing hypersurface to a final uniform-density hypersurface. In the stochastic formalism, the e-folding number is also a stochastic variable labelled \mathcal{N} , which is understood as the *first passage time* to the end of inflation in terms of stochastic calculus. The techniques in stochastic calculus can reveal the statistics of \mathcal{N} and hence ζ , known as the *stochastic- $\delta\mathcal{N}$ approach* [27–29] (see, e.g., Refs. [30–32, 54–81] for its application).

In STOLAS, practically simulations proceed on flat slices and will be stopped well before the end of inflation for all grid points. At that end time, the grid spacing is larger than the

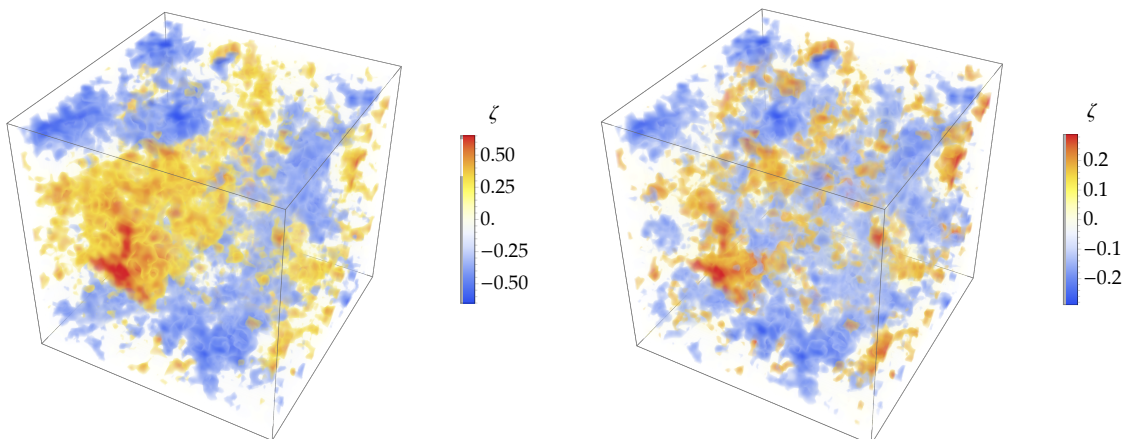


Figure 2. Sample maps of $\zeta(\mathbf{x})$ for the chaotic (left) and Starobinsky's linear (right) models with the parameter sets given in Sec. 3.

Hubble scale. Therefore, one can understand the final configuration of the simulation as an *initial* flat-slicing hypersurface with superHubble fluctuations for the δN scheme. After that, one solves the EoM (2.20) until some final uniform-density slice around the end of inflation⁸ with the independent noise $\xi(N, \mathbf{x})$ for each grid as they are separated further than the Hubble scale and then obtains $\zeta(\mathbf{x})$ for each point as the time fluctuation $\delta N(\mathbf{x})$. One may want to understand $\zeta(\mathbf{x})$ as the coarse-grained curvature perturbation over all the smaller scales than the grid spacing. In that case, letting $\mathcal{N}(\varphi, \varpi)$ the *stochastic* e-folding number from the initial field values (φ, ϖ) to the end hypersurface, the coarse-grained curvature perturbation $\zeta_{\text{cg}}(\mathbf{x})$ is calculated as

$$\zeta_{\text{cg}}(\mathbf{x}) = \langle \mathcal{N}(\varphi(\mathbf{x}), \varpi(\mathbf{x})) \rangle - \overline{\langle \mathcal{N}(\varphi(\mathbf{x}), \varpi(\mathbf{x})) \rangle}, \quad (2.37)$$

where $(\varphi(\mathbf{x}), \varpi(\mathbf{x}))$ are the field values at \mathbf{x} at the end of the simulation, the bracket stands for the ensemble average, and the overline represents the grid average,⁹ $\overline{X(\mathbf{x})} = \frac{1}{N_L^3} \sum_{\mathbf{x}} X(\mathbf{x})$. If one sets the simulation end time so that all grid points are well converged to a slow-roll attractor behaviour as we will do in this paper, the ensemble average can be approximated by the *classical* e-folds N_{cl} obtained without noise:

$$\zeta_{\text{cg}}(\mathbf{x}) \approx N_{\text{cl}}(\varphi(\mathbf{x}), \varpi(\mathbf{x})) - \overline{N_{\text{cl}}(\varphi(\mathbf{x}), \varpi(\mathbf{x}))}. \quad (2.38)$$

We adopt RK4 in the calculation of N_{cl} . Hereafter, we will omit the subscript cg for brevity.

In Fig. 2, we show sample maps of $\zeta(\mathbf{x})$ for two different models described in the following sections in detail. Though we adopt the same noise map in these two models, the resultant $\zeta(\mathbf{x})$ is obviously distinct in both the amplitude and the scale dependence.

⁸Practically, we choose the end slice at the end of inflation $\epsilon_1 = \varpi^2 / (2M_{\text{Pl}}^2 H^2) = 1$ for chaotic inflation and a uniform-inflaton surface for Starobinsky's linear model for simplicity. See Sec. 3.3 for the detailed condition for Starobinsky's linear model.

⁹One may include the volume effect in these averagings. See Ref. [82] for details.

3 Primary statistics

In this section, we check the behaviour of STOLAS by comparing the primary statistics of ζ , the power spectrum and the skewness of the probability density function (PDF), with the standard perturbation theory. We consider two models of inflation: chaotic inflation and Starobinsky's linear potential.

3.1 Calculation of power spectrum

Let us first discuss how to convert the discrete map $\zeta(\mathbf{x})$ obtained in the lattice simulation (see Fig. 2 for example) to the (dimensionless) power spectrum $\mathcal{P}_\zeta(k)$ defined in the continuous Fourier space as usual. The discrete Fourier transformation of ζ is defined similarly to Eq. (2.25) as

$$\zeta_{\mathbf{n}} = \sum_{\mathbf{x}} \zeta(\mathbf{x}) e^{-i\frac{2\pi}{L}\mathbf{n}\cdot\mathbf{x}}, \quad \zeta(\mathbf{x}) = \frac{1}{N_L^3} \sum_{\mathbf{n}} \zeta_{\mathbf{n}} e^{i\frac{2\pi}{L}\mathbf{n}\cdot\mathbf{x}}. \quad (3.1)$$

According to the ergodic theorem, the stochastic average of the one-point variance $\langle \zeta^2(\mathbf{x}) \rangle$ (both in the discrete and the continuous space) can be approximated by the grid-average variance as

$$\langle \zeta^2(\mathbf{x}) \rangle \approx \overline{\zeta^2(\mathbf{x})}. \quad (3.2)$$

The grid-average variance is related to the discrete Fourier mode by

$$\overline{\zeta^2(\mathbf{x})} = \frac{1}{N_L^6} \sum_{\mathbf{n}, \mathbf{m}} \zeta_{\mathbf{n}} \zeta_{\mathbf{m}} \overline{e^{i\frac{2\pi}{L}(\mathbf{n}+\mathbf{m})\cdot\mathbf{x}}} = \frac{1}{N_L^6} \sum_{\mathbf{n}} |\zeta_{\mathbf{n}}|^2, \quad (3.3)$$

where we used $\overline{e^{i\frac{2\pi}{L}(\mathbf{n}-\mathbf{m})\cdot\mathbf{x}}} = \delta_{\mathbf{nm}}$ and the reality condition $\zeta_{-\mathbf{n}} = \zeta_{\mathbf{n}}^*$. On the other hand, the continuous-space variance can be calculated as the integral of the power spectrum in the logarithmic wavenumber,

$$\langle \zeta^2(\mathbf{x}) \rangle = \int_{\ln k_{\min}}^{\ln k_{\max}} d \ln k \mathcal{P}_\zeta(k), \quad (3.4)$$

within the relevant wavenumber range $k \in [k_{\min}, k_{\max}]$. The consistency hence leads to the following relation between the continuous-limit power spectrum and the discrete Fourier mode:

$$\mathcal{P}_\zeta\left(\frac{2\pi}{L}n\right) \approx \frac{1}{N_L^6 \Delta \ln n} \sum_{|\ln m - \ln n| \leq \frac{\Delta \ln n}{2}} |\zeta_{\mathbf{m}}|^2, \quad (3.5)$$

where $\Delta \ln n$ is a certain binning parameter.

3.2 Chaotic inflation

Let us first see the simplest example: chaotic inflation with the quadratic potential,

$$V(\phi) = \frac{1}{2} m^2 \phi^2, \quad (3.6)$$

where m is the mass of the inflaton. We chose the mass and the initial condition of the inflaton as $m = 2.11 \times 10^{-2} M_{\text{Pl}}$ and $(\varphi_i, \varpi_i) = (11 M_{\text{Pl}}, -\sqrt{2/3} m M_{\text{Pl}})$. We have chosen these values that correspond to ~ 30 e-folds before the end of inflation in the classical trajectory because we are interested in small-scale physics in this work. For the single-field slow-roll models such as chaotic inflation, the inflaton's power spectrum as the noise amplitude is calculated up to the next-to-leading order in the slow-roll approximation as¹⁰

$$\mathcal{P}_\phi = \left(\frac{H}{2\pi}\right)^2 \left(\frac{\sigma H}{2H}\right)^{-6\epsilon_V + 2\eta_V} [1 + \epsilon_V(10 - 6\gamma - 12 \ln 2) - 2\eta_V(2 - \gamma - 2 \ln 2)], \quad (3.7)$$

where γ is a Euler's constant (see also Appendix A for detailed derivation). The slow-roll parameters are given by

$$\epsilon_V = \frac{M_{\text{Pl}}^2}{2} \left(\frac{V'}{V}\right)^2, \quad \eta_V = M_{\text{Pl}}^2 \frac{V''}{V}. \quad (3.8)$$

Note that these slow-roll parameters as well as the Hubble parameter should be understood as functions of the field values φ and ϖ at the spatial grid and the time step of interest. $\epsilon_V = \eta_V$ does hold in the quadratic model.

In the left panel of Fig. 3, we show the power spectrum \mathcal{P}_ζ (3.5) at the end of the inflation. We simulate with $N_L^3 = 64^3$ points and the coarse-graining scale $\sigma = 0.1$. The average and the standard error of the power spectrum are estimated with 1000 realisations of the three-dimensional map of curvature perturbation, though the error bars are too small to distinguish. In this plot, the blue points are our simulation results and the black dashed line is the linear-perturbation estimation through the Mukhanov–Sasaki equation. As expected from Fig. 1, while they are scattered for small wavenumbers, the simulation results are well-consistent with the linear perturbation theory for large-enough wavenumbers $n \gtrsim 4$.

We also show the one-point PDF of $\zeta(\mathbf{x})$ in the right panel of Fig. 3. The blue dots show our simulation result and the black dashed line is its Gaussian fitting with the standard deviation $\sigma_\zeta = 0.027$ calculated by the data. The result is almost Gaussian but one can detect small non-Gaussianity, e.g., in terms of the non-linearity parameter defined by

$$f_{\text{NL}} = \frac{5}{18} \frac{\langle \zeta^3(\mathbf{x}) \rangle}{\langle \zeta^2(\mathbf{x}) \rangle^2}, \quad (3.9)$$

equivalent to the standard non-linearity parameter in the local-type assumption [83]. In particular, the so-called Maldacena consistency relation predicts the relation $f_{\text{NL}} = \frac{5}{12}(1 - n_s)$ where $n_s - 1 = d \ln \mathcal{P}_\zeta / d \ln k$ [84]. We numerically evaluate the Mukhanov–Sasaki equation and read the fitting parameters of the power-law assumption $\mathcal{P}_\zeta = A_\zeta n^{n_s - 1}$ as $A_\zeta = 0.007247$ and $n_s = 0.93048$, which means $f_{\text{NL}} = 2.89 \times 10^{-2}$. Our simulation shows $f_{\text{NL}} = (3.06 \pm 0.43) \times 10^{-2}$ which also shows the consistency with the standard perturbation theory as well as the power spectrum.¹¹

¹⁰One sees that it reduces to the standard noise-amplitude $\mathcal{P}_\phi^{1/2} \sim H/(2\pi)$ at the leading-order in the slow-roll approximation ($\epsilon_V, \eta_V \rightarrow 0$). We found that this simple noise amplitude leads to a slightly inconsistent result with the linear perturbation theory. It is necessary to incorporate up to the first order of the slow-roll approximation into the noise amplitude in order for a consistent result within the numerical error.

¹¹It is known that the reproduction of Maldacena's consistency relation requires the cubic correlation both from the δN non-linear mapping and the inflaton's intrinsic non-Gaussianity in the δN formalism (see, e.g., Ref. [85–87]). While the δN non-linear mapping is taken into account by numerically solving the non-linear

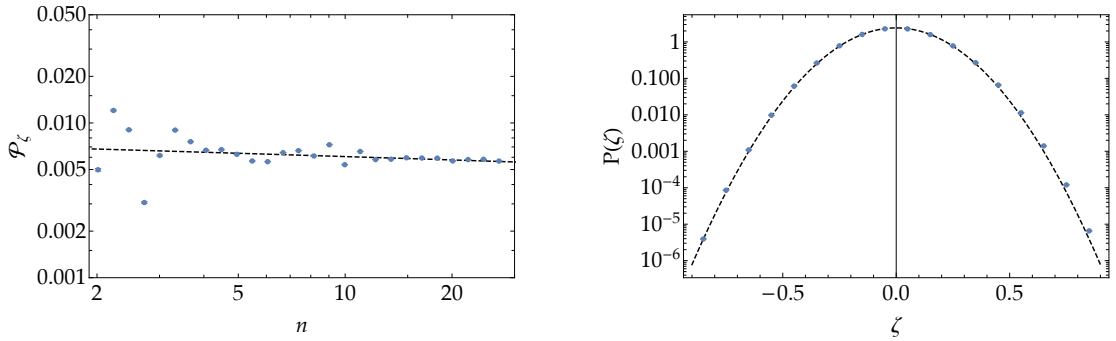


Figure 3. The power spectrum \mathcal{P}_ζ (left) and PDF $P(\zeta)$ (right) of the curvature perturbation in chaotic inflation. We set parameters as $\Delta \ln n = 0.1$, $N_L^3 = 64^3$, and $\sigma = 0.1$. The blue points represent the simulation result, while the black dashed line represents the estimation in the linear perturbation theory through the Mukhanov–Sasaki equation in the left panel and the Gaussian fitting with the standard deviation $\sigma_\zeta \simeq 0.027$ in the right panel.

3.3 Starobinsky’s linear potential

Let us also study Starobinsky’s linear-potential model [91] as a toy model beyond the slow-roll dynamics. The potential is given by

$$V(\phi) = \begin{cases} V_0 + A_+(\phi - \phi_0) & \text{for } \phi > \phi_0, \\ V_0 + A_-(\phi - \phi_0) & \text{for } \phi \leq \phi_0, \end{cases} \quad (3.10)$$

where V_0 and $A_\pm > 0$ are parameters and ϕ_0 is a broken point of potential. If $A_+ > A_-$, the terminal velocity of the inflaton before ϕ_0 is larger than that after ϕ_0 and hence the inflaton experiences the friction-dominated phase called *ultra-slow-roll (USR)* right after ϕ_0 . The USR phase can amplify the curvature perturbation and is compatible with the PBH scenario.

While the noise power is well approximated by $\mathcal{P}_\phi^{1/2} = H/(2\pi)$ in the first stage before ϕ_0 , the slow-roll result (3.7) is not applicable for the second stage after ϕ_0 due to the violation of the slow-roll condition. In the constant Hubble and neglecting noise approximations, the Mukhanov–Sasaki equation has an analytic solution at each phase and can be connected at

EoM, the intrinsic non-Gaussianity seems not as we adopt the Gaussian noise. However, the intrinsic non-Gaussianity in the squeezed limit can actually be understood as the background-dependent noise amplitude [88, 89] and hence we do take its account via the noise amplitude \mathcal{P}_ϕ evaluated at each grid point, which is why we obtained the consistent result with the standard perturbation theory. The equilateral-type non-Gaussianity cannot be included by the Gaussian noise for example, though it is known that that type of non-Gaussianity is negligible in the canonical single-field models (see, e.g., Ref. [90]).

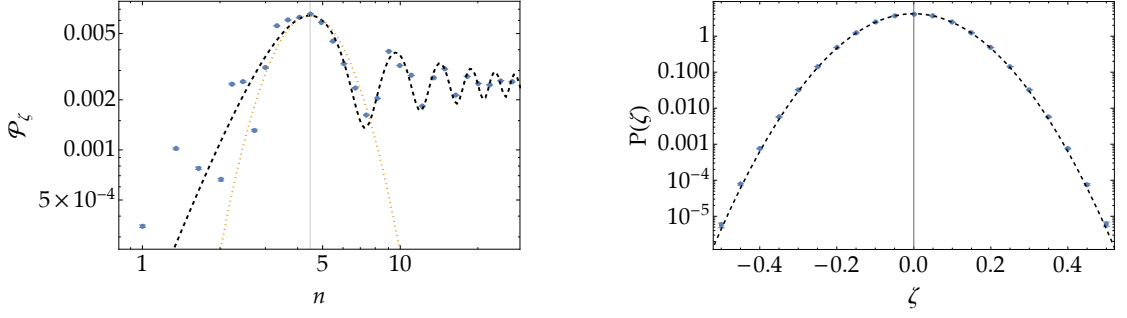


Figure 4. The same plots as Fig. 3 for the Starobinsky’s linear model. The black dashed line represents the analytical formula (3.12) in the linear perturbation theory in the left panel, while it exhibits a Gaussian fitting with the standard deviation $\sigma_\zeta \simeq 0.095$ in the right panel. In the left panel, the black vertical thin line indicates the peak position of the power spectrum, $n_* \simeq 4.47$, and the orange dotted line is a log-normal fitting of the power spectrum about that peak, which are relevant for PBH formation in the next section.

ϕ_0 , which leads to the analytic expression of \mathcal{P}_ϕ for the second stage as (see also Ref. [92])

$$\begin{aligned}
& \mathcal{P}_{\phi,2}(k = \sigma aH) \\
&= \left(\frac{H}{2\pi}\right)^2 \times \frac{1}{2\alpha^6 \Lambda^2 \sigma^6} \left[3(\Lambda^2 (\alpha^4(4\alpha - 7)\sigma^6 + \alpha^3(7\alpha - 16)\sigma^4 + (3 - 12\alpha)\sigma^2 - 3) \right. \\
&\quad + \Lambda(2(5 - 2\alpha)\alpha^4\sigma^6 + 2(14 - 5\alpha)\alpha^3\sigma^4 + 6(4\alpha - 1)\sigma^2 + 6) \\
&\quad \left. - 3(\alpha^4\sigma^6 - (\alpha - 4)\alpha^3\sigma^4 + (4\alpha - 1)\sigma^2 + 1) \cos(2(\alpha - 1)\sigma) \right. \\
&\quad + (\sigma^2 + 1) \left(-18\Lambda(\alpha^2\sigma^2 + 1)^2 + 9(\alpha^2\sigma^2 + 1)^2 + \Lambda^2(2\alpha^6\sigma^6 + 9\alpha^4\sigma^4 + 18\alpha^2\sigma^2 + 9) \right) \\
&\quad \left. + 6\sigma(\alpha^5(\Lambda - 1)\Lambda\sigma^4(\sigma^2 - 1) + \alpha^4(7\Lambda^2 - 10\Lambda + 3)\sigma^4 - \alpha^3(4\Lambda^2 - 7\Lambda + 3)\sigma^2(\sigma^2 - 1) \right. \\
&\quad \left. - 3\alpha(\Lambda - 1)^2(\sigma^2 - 1) - 3(\Lambda - 1)^2 \sin(2\sigma - 2\alpha\sigma) \right], \tag{3.11}
\end{aligned}$$

where $\Lambda := A_+/A_-$, $H \simeq \mathbb{H} \simeq H_0 := \sqrt{V_0/(3M_{\text{Pl}}^2)}$, and $\alpha = \exp(N - \mathcal{N}_0)$ where \mathcal{N}_0 is the transition time: $\varphi(\mathcal{N}_0) = \phi_0$.

In the simulation, we chose the parameters as $H_0 = 10^{-5}M_{\text{Pl}}$, $A_+ = \sqrt{\frac{9H_0^6}{4\pi^2 \times 8.5 \times 10^{-10}}}$, and $A_- = A_+/1700$ and the initial condition as $(\varphi_i, \varpi_i) = (1.93 \times 10^{-2}M_{\text{Pl}}, -5.45 \times 10^{-7}M_{\text{Pl}}^2)$ and set the end surface of the δN formalism at $\phi_{\text{th}} = -1.87 \times 10^{-2}M_{\text{Pl}}$, where the inflaton sufficiently asymptotes to the slow-roll attractor behaviour, supposing that the curvature perturbation gets frozen well regardless of whether inflation ends there or not. In the left panel of Fig. 4, we show the power spectrum with the same lattice setup and plot style as chaotic inflation. For the UV dynamics, we adopt the analytic solution of the Mukhanov–Sasaki equation given by

$$\frac{\mathcal{P}_\zeta(k)}{\mathcal{P}_{\text{IR}}} = \frac{9(\Lambda - 1)^2}{k^6} (\sin k - k \cos k)^4 + \left[\frac{3(\Lambda - 1)}{2k^3} [(k^2 - 1) \sin(2k) + 2k \cos(2k)] + \Lambda \right]^2, \tag{3.12}$$

where our parameter choice corresponds to $\Lambda = 1700$ and $\mathcal{P}_{\text{IR}} = 8.5 \times 10^{-10}$. One again sees their sufficient consistency for $n \gtrsim 4$. In particular, STOLAS works well for the peak value at $n_* \simeq 4.47$ (indicated by the vertical thin line) relevant for the PBH abundance.

In the right panel of Fig. 4, we show the PDF of curvature perturbation with a Gaussian fitting (black dashed) for the standard deviation $\sigma_\zeta = 0.095$. The simulation result is consistent with the Gaussian distribution as $f_{\text{NL}} = (-1.44 \pm 2.77) \times 10^{-3}$.¹² We comment on the so-called exponential-tail feature which has recently attracted attention. For the flat-inflection potential including an USR phase, it is suggested that the probability of large curvature perturbations decays only exponentially rather than the Gaussian decay (see, e.g., Refs. [30, 57, 64]). The non-Gaussian feature represented by this exponential tail in the USR model is sensitive to the end of the USR phase [93, 94]. In our setup, the USR phase smoothly connects with the second slow-roll phase. Such a smooth transition is known to erase the non-Gaussian feature. This is why the simulation result is almost Gaussian. One may add a second breaking point in the potential to force the USR phase to end at that point, and then the exponential-tail feature is expected.

4 Importance sampling for primordial black holes

In this section, we further show the power of STOLAS, simulating the formation of PBHs. The PBHs are hypothetical black holes produced by overdense regions in the radiation-dominated era through gravitational collapse, proposed by Hawking and Carr [95–97] (see also Refs. [98–101] for several reviews). Recently, they have had much motivation from both the theoretical and observational sides. The most famous motivation is the candidate of dark matter (DM). The current observational constraints on PBHs show the window for the whole DM in the mass range $\sim 10^{20}$ g, which corresponds to the subHertz scalar-induced gravitational wave (GW) as an interesting target of the space-based future GW telescopes such as LISA [102], Taiji [103], TianQin [104], and DECIGO [105]. As other motivations, they can explain the seed of supermassive black holes [106], the microlensing events observed by OGLE [107], the hypothetical ninth planet in the solar system [108, 109], the origin of faint supernovae which are the calcium-rich gap transients [110], etc. Subsolar compact objects recently suggested by the observations of the merger GWs are also the interesting possibility of PBHs because the astrophysical BHs cannot be lighter than the solar mass [111–113].

It is suggested that the PBH formation is characterised not only by the absolute value of the curvature perturbation but also its spatial profile (see, e.g., Refs. [33, 34]). STOLAS can get the spatial map of ζ and hence sample the PBH formation in principle. However, the direct sampling of PBHs is non-realistic because PBHs should be extremely rare ($\sim 10\sigma$ rarity, roughly speaking) at their formation time not to overclose the universe. In this paper, we introduce the importance sampling technique (see, e.g., Ref. [35]) to STOLAS to efficiently sample the rare objects.

In this section, we first review the PBH formation in the so-called peak theory. We then introduce the importance sampling method in the context of STOLAS and show some results in the PBH abundance.

4.1 Review of PBH formation

In the radiation-dominated era, basically the subHubble density contrast cannot gravitationally grow due to the radiation pressure. However, if the density contrast is as large as

¹²We do not show the f_{NL} value obtained in the standard perturbation theory because both the power and bispectrum highly depend on the scale and the standard non-linearity parameter is not given by the simple formula (3.9). The value obtained in the simulation should be understood as a mere reference of the Gaussianity of the curvature perturbation.

$\delta_{\text{th}} \sim p/\rho = 1/3$ at the horizon reentry, the gravitational force can overcome the pressure and the overdensity collapses to a BH right after the horizon reentry. The formed BH is called *primordial black hole (PBH)*.¹³ Its mass is roughly given by the horizon mass $M_H = \frac{4\pi}{3}\rho H^{-3}$, which is calculated as (see, e.g., Ref. [131])

$$M_H(k) = 10^{20} \text{ g} \times \left(\frac{g_*}{106.75}\right)^{-1/6} \left(\frac{k}{1.56 \times 10^{13} \text{ Mpc}^{-1}}\right)^{-2}, \quad (4.1)$$

for the horizon reentry of the comoving mode k : $aH/k = 1$. Here, g_* is the effective DoFs for energy density at the horizon reentry and we suppose that it is approximately equivalent to that for entropy.

Since Carr’s simplest criterion $\delta_{\text{th}} \sim 1/3$, the detailed condition of the PBH formation has been investigated both theoretically and numerically. There, the *compaction function* [132, 133], the difference between the Misner–Sharp mass M_{MS} and the expected mass M_{F} in the background universe, or equivalently, the volume average of the density contrast at its horizon reentry, plays a key role. In the spherically symmetric case, it is given by¹⁴

$$\mathcal{C}(r) = 2G \frac{M_{\text{MS}} - M_{\text{F}}}{R} = \frac{2}{3} \left[1 - (1 + r\zeta'(r))^2 \right], \quad (4.2)$$

where r is the comoving radius from the spherical centre and $R(r) = ae^{\zeta(r)}r$ is the corresponding areal radius. According to the latest works [33, 34], the average compaction function defined by

$$\bar{\mathcal{C}}_{\text{m}} = \frac{4\pi \int_0^{R(r_{\text{m}})} \mathcal{C}(r) \tilde{R}^2(r) d\tilde{R}(r)}{\frac{4\pi}{3} R^3(r_{\text{m}})} \quad (4.3)$$

gives a relatively profile-independent criterion, $\bar{\mathcal{C}}_{\text{th}} = 2/5$. Here, r_{m} is the innermost maximum radius of the compaction function.

The numerical simulations in general relativity suggest that the PBH mass follows the scaling behaviour [134–140],

$$M_{\text{PBH}} \simeq K (\bar{\mathcal{C}}_{\text{m}} - \bar{\mathcal{C}}_{\text{th}})^\gamma M_H, \quad (4.4)$$

where K is an order-unity factor, $\gamma \simeq 0.36$ is the universal power index, and M_H is the horizon mass at the horizon reentry $R(r_{\text{m}})H = 1$. We adopt $K = 1$ in this work for simplicity. It is practically useful to rewrite the horizon mass (4.1) in terms of the box size L and the renormalised maximal areal radius $\tilde{R}_{\text{m}} = \frac{N_L}{aL} R(r_{\text{m}}) = \tilde{r}_{\text{m}} e^{\zeta(r_{\text{m}})}$ as

$$M_H(k = r_{\text{m}}^{-1} e^{-\zeta(r_{\text{m}})}) = 2.4 \times 10^{22} \text{ g} \times \left(\frac{g_*}{106.75}\right)^{-1/6} \left(\frac{L}{10^{-12} \text{ Mpc}}\right)^2 \left(\frac{\tilde{R}_{\text{m}}}{N_L}\right)^2. \quad (4.5)$$

¹³Several other mechanisms to produce PBHs have been proposed so far: false-vacuum bubbles [114–122], string-wall networks [123–127], the collapse of isocurvature fluctuations [128, 129], the quark confinement [130], etc.

¹⁴In our notation, the positive ζ corresponds to the overdensity.

The current energy density ratio f_{PBH} of PBHs to total DM in each logarithmic mass bin is defined by

$$f_{\text{PBH}}(M) d \ln M = \frac{M n_{\text{PBH}}(M)}{3M_{\text{pl}}^2 H_0^2 \Omega_{\text{DM}}} d \ln M, \quad (4.6)$$

where Ω_{DM} is the DM density parameter, n_{PBH} is the comoving number density of PBHs, and H_0 is the current Hubble parameter. Below, we calculate the probability $p_t(M) d \ln M$ with which a single PBH within the mass range $\ln M_{\text{PBH}} \in [\ln M - \frac{1}{2} d \ln M, \ln M + \frac{1}{2} d \ln M]$ is realised in the simulation box L^3 , i.e., $n_{\text{PBH}}(M) = p_t(M)/L^3$. One then finds a numerical formula for the PBH abundance:

$$f_{\text{PBH}}(M) = \left(\frac{\Omega_{\text{DM}} h^2}{0.12} \right)^{-1} \left(\frac{M}{10^{20} \text{g}} \right) \left(\frac{L}{10^{-12} \text{Mpc}} \right)^{-3} \left(\frac{p_t(M)}{6.62 \times 10^{-13}} \right), \quad (4.7)$$

where $h = H_0/(100 \text{ km s}^{-1} \text{ Mpc}^{-1})$ is the normalised Hubble parameter.

Let us mention the analytic estimation of the PBH abundance so far. Recently, the so-called peak theory [141] has attracted attention as the state-of-art scheme for the PBH abundance estimation [142–145].¹⁵ If the curvature perturbation is well approximated by a Gaussian random field, the probability of any configuration of $\zeta(\mathbf{x})$ can be determined only by its power spectrum in principle. In particular, if the power spectrum is monochromatic as

$$\mathcal{P}_\zeta(k) = A_s \delta(\ln k - \ln k_*), \quad (4.8)$$

with the amplitude A_s and the characteristic scale k_* , the estimation becomes much simpler. For example, the rare peak is typically fit by the spherically symmetric profile,

$$\hat{\zeta}(r) = \tilde{\mu}_2 \text{sinc}(k_* r), \quad (4.9)$$

with the Gaussian random amplitude μ_2 . The expected PBH number density reads¹⁶

$$n_{\text{PBH}}^{\text{peak}}(M) d \ln M = \frac{k_*^3}{(6\pi)^{3/2}} f\left(\frac{\tilde{\mu}_2}{\sqrt{A_s}}\right) P_G(\tilde{\mu}_2, A_s) \left| \frac{d \ln M}{d \tilde{\mu}_2} \right|^{-1} d \ln M, \quad (4.10)$$

with the function $f(\xi)$,

$$f(\xi) = \frac{1}{2} \xi (\xi^2 - 3) \left(\text{erf} \left[\frac{1}{2} \sqrt{\frac{5}{2}} \xi \right] + \text{erf} \left[\sqrt{\frac{5}{2}} \xi \right] \right) + \sqrt{\frac{2}{5\pi}} \left\{ \left(\frac{8}{5} + \frac{31}{4} \xi^2 \right) \exp \left[-\frac{5}{8} \xi^2 \right] + \left(-\frac{8}{5} + \frac{1}{2} \xi^2 \right) \exp \left[-\frac{5}{2} \xi^2 \right] \right\}, \quad (4.11)$$

the Gaussian PDF $P_G(x, \sigma^2) = \frac{1}{\sqrt{2\pi\sigma^2}} e^{-x^2/(2\sigma^2)}$, and the $\tilde{\mu}_2$ -dependence of the PBH mass numerically found as¹⁷

$$\left| \frac{d \ln M}{d \tilde{\mu}_2} \right| = \left| 2 \frac{d \hat{\zeta}(r_m)}{d \tilde{\mu}_2} + \frac{\gamma}{\tilde{\mu}_2 - \tilde{\mu}_{2,\text{th}}} \right| \simeq 0.282 + \frac{0.36}{\tilde{\mu}_2 - \tilde{\mu}_{2,\text{th}}}, \quad (4.12)$$

¹⁵See also, e.g., Refs. [146, 147] for other recent statistical approaches to the PBH abundance.

¹⁶Note that the expression in the original work [142] suffers from the extra factor of 27, which propagated to several literatures. It is fixed in our expression.

¹⁷Note that the scaling behaviour of the PBH mass with respect to the amplitude $\tilde{\mu}_2$ is used to derive this relation in Ref. [145], which results in a mere difference of the prefactor K .

where $\tilde{\mu}_{2,\text{th}} \simeq 0.615$ is the PBH formation threshold for the profile (4.9). The PBH abundance is hence estimated as

$$f_{\text{PBH}}^{\text{peak}}(M) = \left(\frac{\Omega_{\text{DM}} h^2}{0.12}\right)^{-1} \left(\frac{M}{10^{20} \text{ g}}\right) \left(\frac{k_*}{1.56 \times 10^{13} \text{ Mpc}^{-1}}\right)^3 \times \left(\frac{\left|\frac{d \ln M}{d \tilde{\mu}_2}\right|^{-1} f\left(\frac{\tilde{\mu}_2(M)}{\sqrt{A_s}}\right) \text{P}_G(\tilde{\mu}_2(M), A_s)}{1.4 \times 10^{-14}}\right). \quad (4.13)$$

Below, we compare the result in our STOLAS with this analytic formula.

4.2 Importance sampling

The direct sampling of PBHs is non-realistic as they should be extremely rare. We here introduce the importance sampling technique to STOLAS (see Ref. [35] for its application to the stochastic- $\delta\mathcal{N}$ formalism). The simulation of the stochastic process is realised by numerically generating the stochastic noise. Given the probability distribution of the noise, one can conversely introduce *intentionally* large noise whose true probability is calculable as well. In this way, one can sample overdensities much more efficiently and correct the obtained histogram to follow the true probability distribution.

In this work, we introduce an offset $\mathcal{B}(N, \mathbf{x})\Delta N$ called *bias* to the stochastic noise $\Delta W(N, \mathbf{x})$ as

$$\begin{aligned} \varphi(N + \Delta N, \mathbf{x}) - \varphi(N, \mathbf{x}) &= \frac{\varpi(N, \mathbf{x})}{H(N, \mathbf{x})} \Delta N + \mathcal{P}_\phi^{1/2}(N, k_\sigma(N))(\mathcal{B}(N, \mathbf{x})\Delta N + \Delta W(N, \mathbf{x})), \\ \varpi(N + \Delta N, \mathbf{x}) - \varpi(N, \mathbf{x}) &= \left(-3\varpi(N, \mathbf{x}) - \frac{V'(\varphi(N, \mathbf{x}))}{H(N, \mathbf{x})}\right) \Delta N. \end{aligned} \quad (4.14)$$

Respecting the typical profile (4.9), we adopt the sinc spatial dependence around the origin at about the time of interest N_b as

$$\mathcal{B}(N, \mathbf{x}) = B(N)S(N, \mathbf{x}), \quad \begin{cases} B(N) = \frac{b}{\sqrt{2\pi}\Delta N_b} \exp\left(-\frac{(N-N_b)^2}{2(\Delta N_b)^2}\right), \\ S(N, \mathbf{x}) = \text{sinc}(k_\sigma(N)x), \end{cases} \quad (4.15)$$

where b is the overall amplitude parameter and ΔN_b controls the duration of the bias around N_b . According to the discussion in Sec. 2.2, the sinc function can be represented by the superposition of the Fourier modes in the shell $\zeta(N)$ as

$$S(N, \mathbf{x}) \simeq \frac{1}{|\zeta(N)|} \sum_{\mathbf{n} \in \zeta(N)} e^{i\frac{2\pi}{L}\mathbf{n}\cdot\mathbf{x}}. \quad (4.16)$$

Hence the biased EoM (4.14) is equivalent to replacing the Fourier-space noise as $\Delta W_{\mathbf{n}}(N) \rightarrow \Delta W_{\mathbf{n}}(N) + \frac{N_b^3}{|\zeta(N)|} B(N)\Delta N$. Appropriately choosing the amplitude b , maps realising PBHs around the origin can be sampled more efficiently.

Though the biased EoM is different from the original one, the realised samples by this equation denoted $\omega \in \Omega$ in the sample space Ω can be the solutions of the original one in principle if the whole shifted noise $\Delta W_{\mathbf{n}}(N) + \frac{N_b^3}{|\zeta(N)|} B(N)\Delta N$ is realised by the original distribution (2.34). Only its realisation probability is different: ω is realised with the *sampling*

probability $p_s(\omega)$ by the biased EoM, while the true *target probability* $p_t(\omega)$ is associated with the original EoM. As $p_s(\omega)$ can be estimated by the numerical histogram, the target probability $p_t(\omega)$ can be obtained by calculating the *weight function* defined by

$$\mathcal{W}(\omega) = \frac{p_t(\omega)}{p_s(\omega)}. \quad (4.17)$$

The sampling probability of ω is the realisation probability of the noise $\Delta W_{\mathbf{n}}$ as $p_s(\omega) = p(\{\Delta W_{\mathbf{n}}(N)\} | \omega)$, while ω is realised by the shifted noise in the true system, i.e., $p_t(\omega) = p\left(\left\{\Delta W_{\mathbf{n}}(N) + \frac{N_L^3}{|\varsigma(N)|} B(N) \Delta N\right\} | \omega\right)$. Recalling the noise distribution (2.34), the (log of) weight function is hence calculated as

$$\ln \mathcal{W}(\omega) = \sum_N \ln w(N), \quad (4.18)$$

where

$$\begin{aligned} \ln w(N) &= - \sum_{\mathbf{n} \in \mathcal{C} \cap \varsigma(N)} \frac{\left| \Delta W_{\mathbf{n}}(N) + \frac{N_L^3}{|\varsigma(N)|} B(N) \Delta N \right|^2 - |\Delta W_{\mathbf{n}}(N)|^2}{\frac{N_L^6}{|\varsigma(N)|} \Delta N} \\ &\quad - \sum_{\mathbf{n} \in \mathcal{R} \cap \varsigma(N)} \frac{\left(\Delta W_{\mathbf{n}}(N) + \frac{N_L^3}{|\varsigma(N)|} B(N) \Delta N \right)^2 - (\Delta W_{\mathbf{n}}(N))^2}{2 \frac{N_L^6}{|\varsigma(N)|} \Delta N} \\ &= - \frac{B(N)}{N_L^3} \sum_{\mathbf{n}} \Delta W_{\mathbf{n}}(N) - \frac{1}{2} B^2(N) \Delta N \\ &= -B(N) \Delta W(N, \mathbf{x} = \mathbf{0}) - \frac{1}{2} B^2(N) \Delta N. \end{aligned} \quad (4.19)$$

Here we used $2|\mathcal{C} \cap \varsigma| + |\mathcal{R} \cap \varsigma| = |\varsigma|$, $\Delta W_{\mathbf{n}} = 0$ for $\mathbf{n} \notin \varsigma$, and $\sum_{\mathbf{n}} \text{Re}[\Delta W_{\mathbf{n}}] = \sum_{\mathbf{n}} \Delta W_{\mathbf{n}}$. This is a Gaussian variable of the average and variance given by

$$\begin{aligned} \langle \ln \mathcal{W} \rangle &= -\frac{1}{2} \sum_N B^2(N) \Delta N \simeq -\frac{1}{2} \int B^2(N) dN \simeq -\frac{b^2}{4\sqrt{\pi} \Delta N_b}, \\ \langle (\ln \mathcal{W} - \langle \ln \mathcal{W} \rangle)^2 \rangle &= \sum_N B^2(N) \Delta N \simeq \int B^2(N) dN \simeq \frac{b^2}{2\sqrt{\pi} \Delta N_b}. \end{aligned} \quad (4.20)$$

Dividing the samples into bins as $\Omega = \bigcup_i \Omega_i$ with respect to quantities of interest, the sampling probability is evaluated by the histogram as

$$p_s(\Omega_i) \approx \frac{|\Omega_i|}{|\Omega|}. \quad (4.21)$$

The target probability is then obtained by multiplying it by the average weight in the corresponding bin:

$$p_t(\Omega_i) = \langle \mathcal{W}(\omega \in \Omega_i) \rangle p_s(\Omega_i). \quad (4.22)$$

Practically, the average weight is difficult to be estimated by the direct sample average as the weight varies by many orders of magnitude. Rather the log of the weight can be expected to

well follow the Gaussian distribution in each bin like as the unbinned one (4.19). Supposing its lognormal distribution, the average weight can be estimated more accurately by the log average and variance within the propagated error as (see Ref. [35])

$$\langle \mathcal{W}(\omega \in \Omega_i) \rangle = \exp \left(\overline{\ln \mathcal{W}_i} + \frac{\sigma_{\ln \mathcal{W}_i}^2}{2} \right) \left| \exp \left[\pm \sqrt{\frac{\sigma_{\ln \mathcal{W}_i}^2}{|\Omega_i|} + \frac{\sigma_{\ln \mathcal{W}_i}^4}{2|\Omega_i| - 2}} \right] - 1 \right|, \quad (4.23)$$

where

$$\overline{\ln \mathcal{W}_i} = \frac{1}{|\Omega_i|} \sum_{\omega \in \Omega_i} \ln \mathcal{W}(\omega), \quad \sigma_{\ln \mathcal{W}_i}^2 = \frac{1}{|\Omega_i| - 1} \sum_{\omega \in \Omega_i} (\ln \mathcal{W}(\omega) - \overline{\ln \mathcal{W}_i})^2. \quad (4.24)$$

We stress that the choice of the bias form (4.9) does not change the final result such as the PBH abundance but only affects the sampling efficiency. A wrong choice of the bias merely reduces the efficiency and enlarges the sampling errors but the infinite sampling anyway leads to the true statistics. The validity of the bias choice can be indicated by the correlation between the weight value and the quantity of interest such as the left panel of Fig. 6.

4.3 Results and Discussion

Let us see the results of the importance sampling in Starobinsky's linear model with the same parameters discussed in Sec. 3.3. We adopt the box size $L = 10^{-12}$ Mpc and $(b, N_b, \Delta N_b) = (20\sqrt{\Delta N_b}, 3.8, 0.1)$ for the bias parameters in Eq. (4.15), where N_b corresponds to the peak wave number $n_* = 4.47$ of the power spectrum shown in Fig. 4 via the cutoff scale $n_\sigma(N_b) = \sigma e^{N_b}$. In Fig. 5, we show two sample xy -slices at $z = 0$ of the biased ζ contour map for a PBH-forming $\bar{\mathcal{C}}_m > 2/5$ realisation and not $\bar{\mathcal{C}}_m < 2/5$. The corresponding spherical-average profile $\zeta(\tilde{r})$ and numerically obtained compaction function $\mathcal{C}(\tilde{r})$ (4.2) as functions of the normalised radius $\tilde{r} = \frac{N_L}{L} |\mathbf{x}|$ are compared with the correspondings of the sinc profile (4.9). They are consistent around the peak for the PBH-forming realisation as the power spectrum is well peaked around $n_\sigma(N_b)$ and the curvature perturbation is almost Gaussian.

The left panel of Fig. 6 shows the density histogram in the average compaction function $\bar{\mathcal{C}}_m$ (4.3) and the weight function \mathcal{W} (4.19). Their negative correlation indicates that larger overdensities are rarer as expected and the choice of the bias function (4.15) works well. For PBH-forming maps $\bar{\mathcal{C}}_m > 2/5$, the corresponding PBH mass M_{PBH} can be calculated by Eq. (4.5) with the computed $\bar{\mathcal{C}}_m$ and R_m and then one finds the density histogram in M_{PBH} and \mathcal{W} as shown in the right panel of Fig. 6. Through the lognormal estimator (4.23), it converts the sampling probability p_s by the histogram (4.21) (the left panel of Fig. 7) into the target probability p_t shown in the right panel of Fig. 7. It is directly followed by the current PBH mass function f_{PBH} via the formula (4.7). Our final result is shown in Fig. 8 with the prediction of the peak theory as a comparison. Here, the peak theory calculation is done by first fitting the peak of the power spectrum by the log-normal function (the orange-dotted line in the left panel of Fig. 4) and approximating it by the Dirac delta function (4.8) with the same amplitude $A_s = 5.054 \times 10^{-3}$. Despite their completely independent approaches, the amplitude and scale dependence of their independent result are roughly consistent with the known analytical calculation, indicating that STOLAS with the importance sampling technique works. The quantitative difference would be caused by the monochromatic power spectrum assumption (4.8) in the peak theory or the low spatial resolution of STOLAS, which we leave for future work.

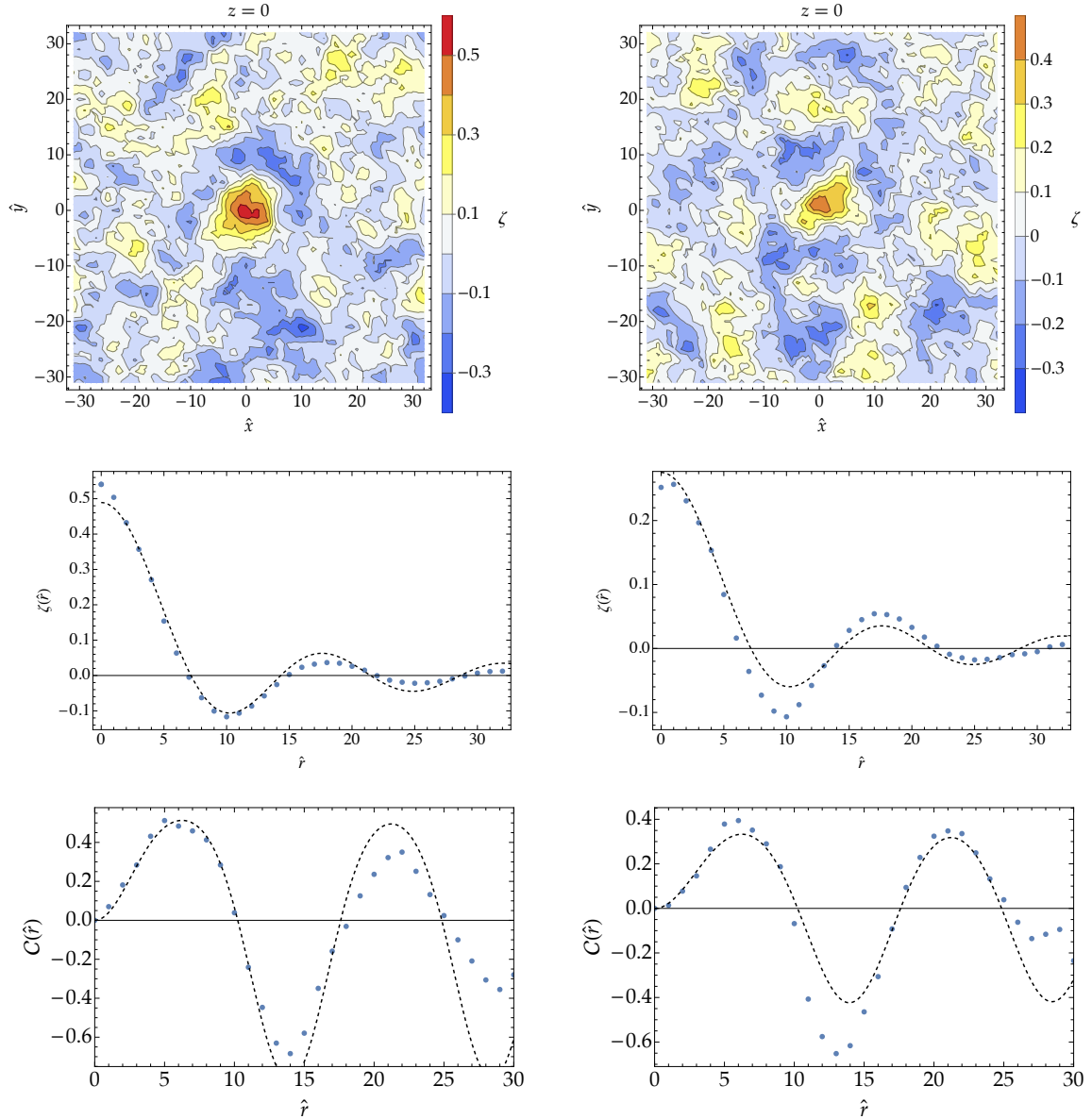


Figure 5. Samples of the contours of ζ for the $z = 0$ slice (top), the corresponding radial profile $\zeta(\hat{r})$ (middle), and the compaction function $\mathcal{C}(\hat{r})$ (bottom) for Starobinsky’s linear model. The left panels correspond to a PBH-forming realisation $\bar{C}_m > 2/5$, while the right panels are for a non-PBH-forming one $\bar{C}_m < 2/5$. In the middle and bottom panels, the blue dots are the numerical results and the black-dashed lines represent the sinc-profile fitting with $n_\sigma(N_b)$.

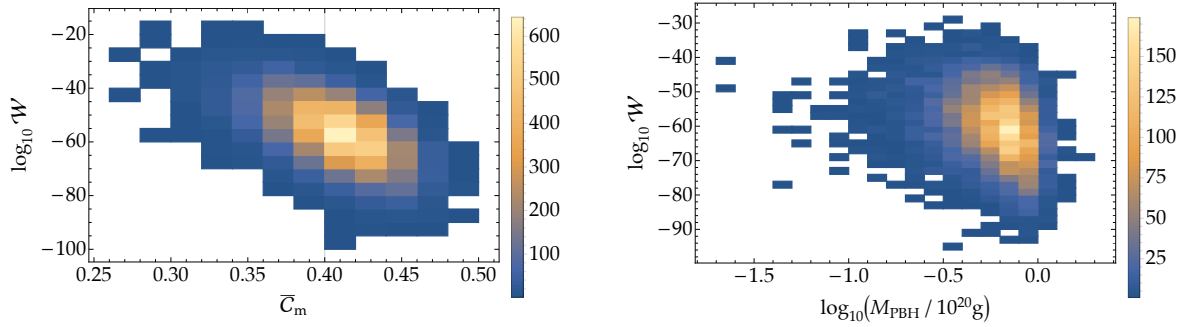


Figure 6. *Left:* the density histogram of the average compaction function \bar{C}_m (4.3) and the weight function \mathcal{W} (4.19) of the 10000 samples for Starobinsky’s linear model. Thanks to the bias, the PBH-forming maps $\bar{C}_m \simeq \bar{C}_{\text{th}} = 2/5$ (shown by the vertical thin line) are intensively realised. The negative correlation between \bar{C}_m and \mathcal{W} indicates that larger overdensities are rarer as expected. *Right:* the same plot with respect to the PBH mass M_{PBH} (4.5) and the weight for 6396 samples for which \bar{C}_m exceeds the threshold $\bar{C}_{\text{th}} = 2/5$.

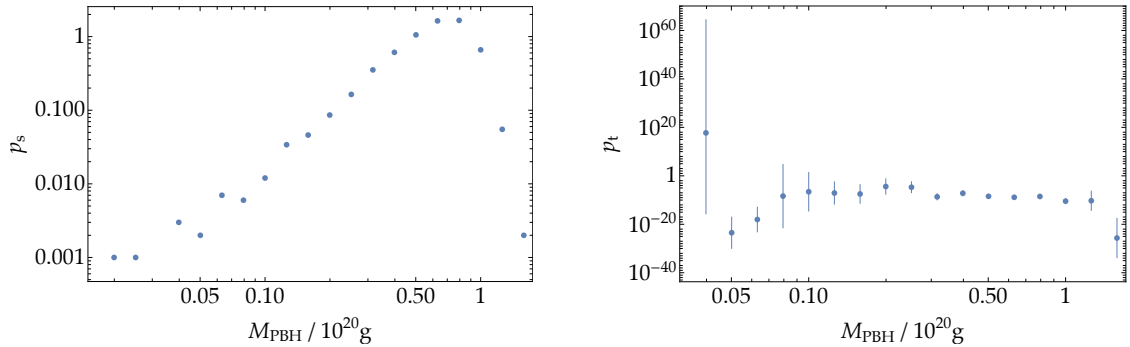


Figure 7. The sampling probability p_s (left) and the target probability p_t (right) with respect to the PBH mass.

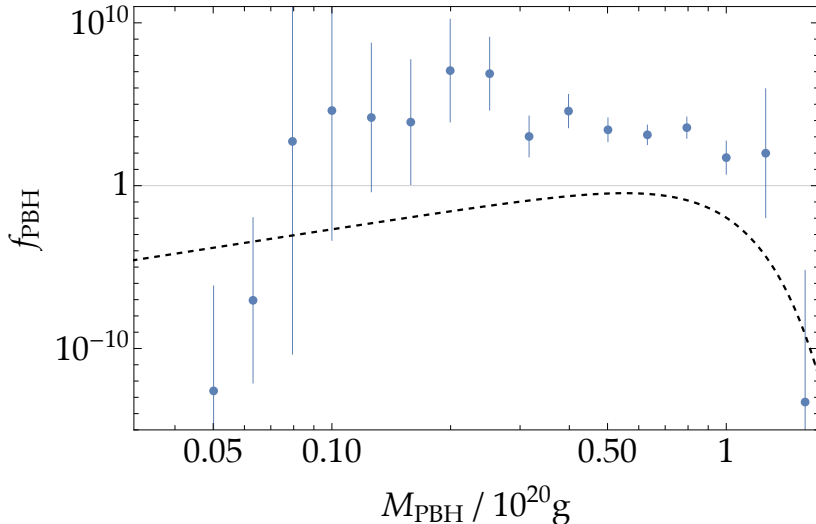


Figure 8. The total PBH abundance f_{PBH} for Starobinsky’s linear model. We adopt $g_* = 106.75$ and $\Omega_{\text{DM}} h^2 = 0.12$ [148]. The blue dots with error bars are the numerical results, while the black-dashed line is the estimation of the peak theory in the monochromatic assumption (4.8) at $n_\sigma(N_b) \simeq 4.47$ with the amplitude $A_s = 5.054 \times 10^{-3}$.

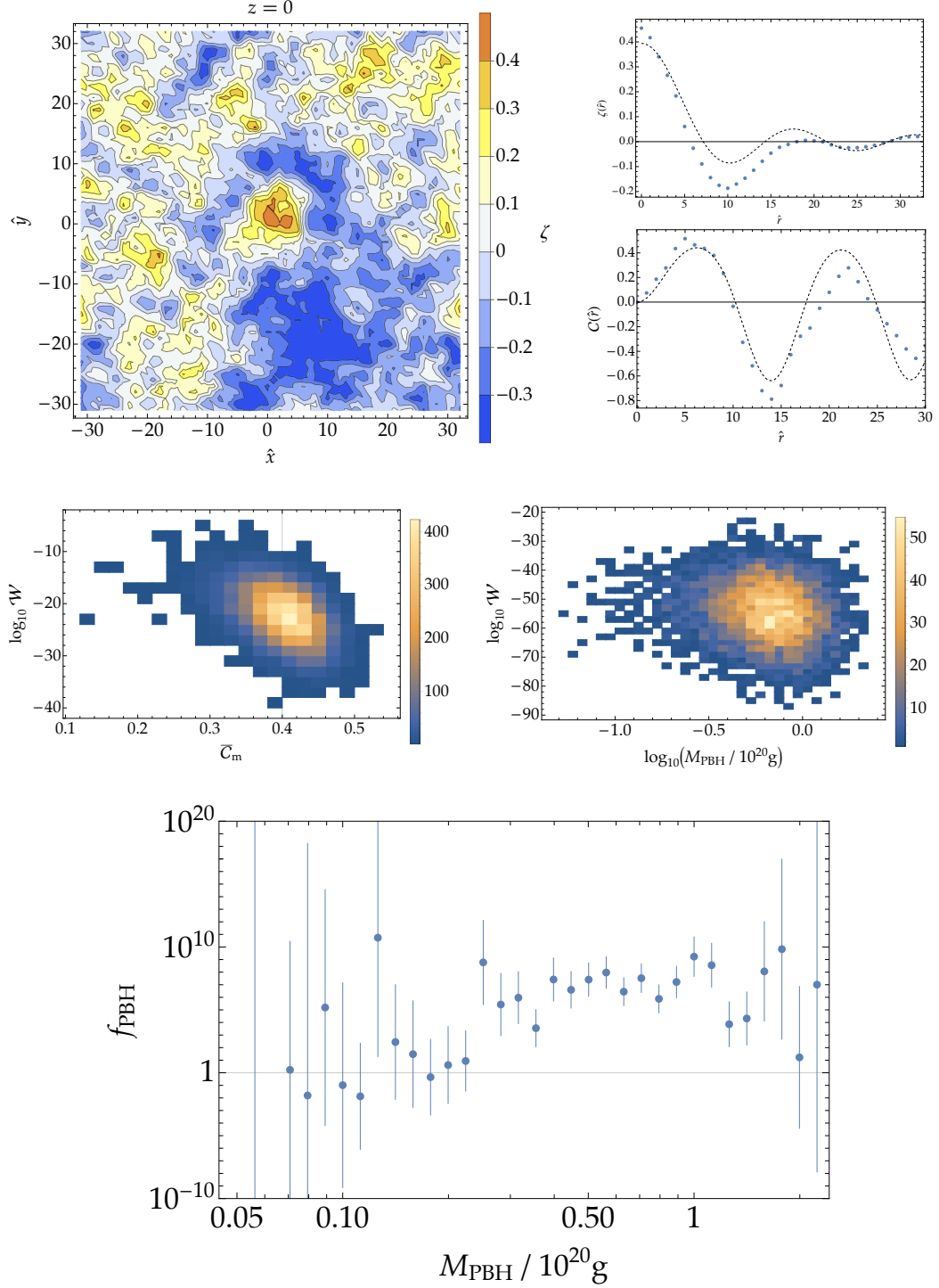


Figure 9. The same plots as Figs. 5–8 for chaotic inflation. The same noise map is used for the top panels as the left panels of Fig. 5.

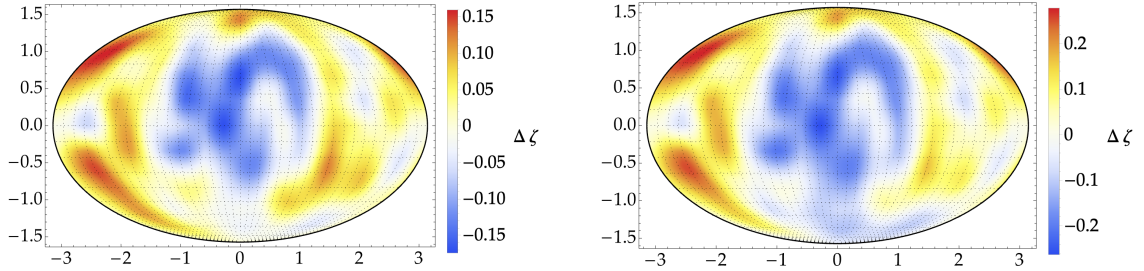


Figure 10. Examples of the angular dependence of the curvature perturbation around the spherical average, $\Delta\zeta$, at $\hat{r} = 3.6$ corresponding to the quarter wave $N_L/(4n_\sigma(N_b))$. The left panel is for Starobinsky’s linear model while the right is for chaotic inflation. We use the same noise map. One finds that the broader power spectrum in chaotic inflation causes a more non-spherical overdensity, which may affect the PBH formation criterion.

The results for chaotic inflation are shown in Fig. 9.¹⁸ One can find a broad feature of the mass function reflecting the nearly scale-invariant power spectrum shown in Fig. 3 though the bias is introduced only for a specific scale $\sim n_\sigma(N_b)$. It is enabled by the randomly added noise $\Delta W(N, \mathbf{x})$. One can extract f_{PBH} for different masses more accurately by changing the bias time N_b .

We mention a caveat in this result. As shown in Fig. 10, chaotic inflation generates more non-spherical overdensities due to its broad power spectrum. In fact, we calculated the angular power spectrum

$$C_\ell = \frac{1}{2\ell + 1} \sum_{m=-\ell}^{+\ell} |a_{\ell m}|^2, \quad a_{\ell m} = \int \zeta(\Omega) Y_\ell^m(\Omega) d\Omega, \quad (4.25)$$

where $Y_\ell^m(\Omega)$ is the spherical harmonics and found $C_1 = (1.095 \pm 0.009) \times 10^{-2}$ and $C_2 = (3.123 \pm 0.020) \times 10^{-3}$ for Starobinsky’s linear model while $C_1 = (2.112 \pm 0.017) \times 10^{-2}$ and $C_2 = (6.415 \pm 0.040) \times 10^{-3}$ for chaotic inflation at the quarter wave $\hat{r} = N_L/(4n_\sigma(N_b)) \simeq 3.6$ where the standard errors are estimated with 10,000 samples. Large non-sphericity may cause a wrong judgement of PBH formation with the spherical compaction function criterion as indicated by the worse fitting of the sinc profile or the less correlation between \mathcal{W} and \bar{C}_m in Fig. 9. We leave it for future work.

5 Conclusions

In this paper, we proposed the C++ package, STOCHASTIC LATTICE SIMULATION (STOLAS), of cosmic inflation. It simulates the dynamics of the inflaton fields in the manner of the stochastic formalism, the effective theory of superHubble fields, and calculates the observable curvature perturbation according to the δN formalism. In Sec. 2, we described the implementation of STOLAS by discretising the stochastic formalism. In Sec. 3, we calculated primary statistics such as the power spectrum and the non-linearity parameter of the curvature perturbation in two toy models: chaotic inflation and Starobinsky’s linear-potential inflation. The results (Figs. 3 and 4) show the consistency of STOLAS with the standard perturbation theory in the perturbative observables. As a further application of STOLAS

¹⁸The peak theory result is not shown because the calculation for the nearly scale-invariant or broad power spectrum with the average compaction criterion has not been given in the literature.

beyond the perturbative quantities, we calculated the abundance of PBHs in the two models in Sec. 4 by introducing the technique of the importance sampling, which can efficiently sample rare events such as PBHs. For the first time, we had success in directly sampling the PBH abundance f_{PBH} in a full numerical way as shown in Figs. 8 and 9. The quantitative inconsistency between STOLAS and the analytic result in the peak theory may be caused by the monochromatic power spectrum approximation in the peak theory and/or the low spatial resolution of STOLAS. We leave a detailed analysis of this inconsistency for future work.

The simulation reveals that the non-sphericity of the overdensity tends to be relatively large for a broader power spectrum represented by chaotic inflation (Fig. 10). It will hence be interesting to investigate the PBH formation criteria for a non-spherical overdensity in numerical relativity (see, e.g., Ref. [149] for such an attempt). Also, while the non-Gaussianity of the curvature perturbation is small in both models we consider, particularly in Starobinsky’s linear model because the end of USR phase is smoothly connected to the second slow-roll phase in our setup, one may introduce a sharp transition from USR to slow-roll which is known to cause the *exponential-tail* feature in the curvature perturbation. This non-perturbative feature can significantly enhance the PBH abundance and therefore be a good target of the investigation with STOLAS. Multifield extensions such as hybrid inflation (see, e.g., Refs. [54, 80, 150]) are also attractive as they predict non-Gaussian curvature perturbations in general (see, e.g., Refs. [151–154] in the context of hybrid inflation).

STOLAS’s application is not limited to the PBH. The map of the curvature perturbations obtained in STOLAS could be used as the initial condition of the structure formation simulation such as N -body simulations. Since it does not require translating the information of the curvature perturbation into small numbers of statistics such as the power or bispectrum, one can extract the full non-perturbative features of the curvature perturbation embedded into the large-scale structure (see, e.g., Ref. [70] for the effect of the exponential tail to the number of massive clusters).

Acknowledgments

We are grateful to Takashi Hiramatsu, Naoya Kitajima, and Shuichiro Yokoyama for their helpful discussions, and to Angelo Caravano, Diego Cruces, Albert Escrivà, Cristiano Germani, Rhodai Kawaguchi, Eiichiro Komatsu, Lucas Pinol, Koki Tokeshi, and Vincent Vennin, Edoardo Vitagliano for their useful comments on the draft. We also thank the organisers and participants of *Observational Cosmology Summer Workshop in 2022*, where the key idea of the work was given. This work is supported by JSPS KAKENHI Grants No. JP23KJ2007 (T.M.), No. JP21K13918 (Y.T.), and No. JP24K07047 (Y.T.).

A Derivation of the power spectrum of the scalar field at NLO in slow-roll

In this appendix, we derive the power spectrum of the scalar field up to the next-to-leading order (NLO) in the slow-roll expansion. Note that we ignore the noise term throughout this appendix. Following Ref. [155], the slow-roll parameters are given by

$$\epsilon_1 = -\frac{\dot{H}}{H^2}, \quad \epsilon_2 = \frac{\dot{\epsilon}_1}{H\epsilon_1}. \quad (\text{A.1})$$

The relationship between the conformal time and the comoving horizon is calculated as

$$aH \simeq -\frac{1}{7}(1 + \epsilon_1). \quad (\text{A.2})$$

The Mukhanov–Sasaki equation for the canonicalised inflaton perturbation $v = a\delta\phi$ is given by

$$\frac{\partial^2 v}{\partial \tau^2} + \left(k^2 - \frac{1}{z} \frac{\partial^2 z}{\partial \tau^2} \right) v = 0, \quad (\text{A.3})$$

where $z = a\dot{\phi}/H$. We can express the last term by using slow-roll parameters as

$$\frac{1}{z} \frac{\partial^2 z}{\partial \tau^2} \simeq \frac{1}{\tau^2} \left(2 + 3\epsilon_1 + \frac{3}{2}\epsilon_2 \right). \quad (\text{A.4})$$

Supposing the slow-roll parameters are almost constant up to NLO, Eq. (A.3) can be solved analytically as

$$v(\tau) = \sqrt{\frac{\pi}{4k}} e^{i\pi(\nu+1/2)/2} \sqrt{-k\tau} H_\nu^{(1)}(-k\tau), \quad (\text{A.5})$$

where $H_\nu^{(1)}(x)$ is the Hankel Function of the First Kind, and the parameter ν is given by

$$\nu \simeq \frac{3}{2} + \epsilon_1 + \frac{1}{2}\epsilon_2. \quad (\text{A.6})$$

Here, we chose the integration constant consistent with the adiabatic vacuum in the sub-Hubble limit. The asymptotic form of the Hankel function in the superHubble limit is given by

$$H_\nu^{(1)}(x) \rightarrow -i \frac{\Gamma(\nu)}{\pi} \left(\frac{2}{x} \right)^2, \quad (\text{A.7})$$

where the Gamma function $\Gamma(\nu)$ is expanded as

$$\Gamma(\nu) \simeq \Gamma\left(\frac{3}{2}\right) \left[1 + \left(\epsilon_1 + \frac{1}{2}\epsilon_2 \right) (2 - \gamma - 2 \ln 2) \right] \quad (\text{A.8})$$

with the Euler's constant γ . Using these relations, the power spectrum of ϕ is computed as

$$\begin{aligned} \mathcal{P}_\phi(\sigma a H) &= \frac{k^3}{2\pi a^2} \frac{-\tau}{4} \left| H_\nu^{(1)}(-k\tau) \right|^2 \\ &= \left(\frac{H}{2\pi} \right)^2 [1 + 2\epsilon_1(1 - \gamma - 2 \ln 2) + \epsilon_2(2 - \gamma - 2 \ln 2)] \left(\frac{\sigma H}{2H} \right)^{-2\epsilon_1 - \epsilon_2}. \end{aligned} \quad (\text{A.9})$$

One can change the slow-roll parameters to the potential form with the use of the relation

$$\epsilon_V = \frac{M_{\text{Pl}}^2}{2} \frac{V'}{V} \simeq \epsilon_1, \quad \eta_V = M_{\text{Pl}}^2 \frac{V''}{V} \simeq 2\epsilon_1 - \frac{1}{2}\epsilon_2. \quad (\text{A.10})$$

Then, the power spectrum is written as

$$\mathcal{P}_\phi(\sigma a H) = \left(\frac{H}{2\pi} \right)^2 [1 + \epsilon_V(10 - 6\gamma - 12 \ln 2) - 2\eta_V(2 - \gamma - 2 \ln 2)] \left(\frac{\sigma H}{2H} \right)^{-6\epsilon_V + 2\eta_V}. \quad (\text{A.11})$$

Practically, this form is more useful because the second time derivative in ϵ_2 is not well defined in the stochastic system.

References

- [1] A. A. Starobinsky, *A New Type of Isotropic Cosmological Models Without Singularity*, *Phys. Lett. B* **91** (1980) 99.
- [2] K. Sato, *First-order phase transition of a vacuum and the expansion of the Universe*, *Mon. Not. Roy. Astron. Soc.* **195** (1981) 467.
- [3] A. H. Guth, *The Inflationary Universe: A Possible Solution to the Horizon and Flatness Problems*, *Phys. Rev. D* **23** (1981) 347.
- [4] A. D. Linde, *A New Inflationary Universe Scenario: A Possible Solution of the Horizon, Flatness, Homogeneity, Isotropy and Primordial Monopole Problems*, *Phys. Lett. B* **108** (1982) 389.
- [5] A. Albrecht and P. J. Steinhardt, *Cosmology for Grand Unified Theories with Radiatively Induced Symmetry Breaking*, *Phys. Rev. Lett.* **48** (1982) 1220.
- [6] A. D. Linde, *Chaotic Inflation*, *Phys. Lett. B* **129** (1983) 177.
- [7] PLANCK collaboration, Y. Akrami et al., *Planck 2018 results. X. Constraints on inflation*, *Astron. Astrophys.* **641** (2020) A10 [[1807.06211](#)].
- [8] M. Vogelsberger, F. Marinacci, P. Torrey and E. Puchwein, *Cosmological Simulations of Galaxy Formation*, *Nature Rev. Phys.* **2** (2020) 42 [[1909.07976](#)].
- [9] A. Caravano, E. Komatsu, K. D. Lozanov and J. Weller, *Lattice simulations of inflation*, *JCAP* **12** (2021) 010 [[2102.06378](#)].
- [10] A. Caravano, E. Komatsu, K. D. Lozanov and J. Weller, *Lattice simulations of Abelian gauge fields coupled to axions during inflation*, *Phys. Rev. D* **105** (2022) 123530 [[2110.10695](#)].
- [11] A. Caravano, E. Komatsu, K. D. Lozanov and J. Weller, *Lattice simulations of axion- $U(1)$ inflation*, *Phys. Rev. D* **108** (2023) 043504 [[2204.12874](#)].
- [12] A. Caravano, *Simulating the inflationary Universe: from single-field to the axion- $U(1)$ model*, Ph.D. thesis, Munich U., Munich U., 7, 2022. [2209.13616](#). [10.5282/edoc.30905](#).
- [13] D. G. Figueroa, J. Lizarraga, A. Urrio and J. Urrestilla, *Strong Backreaction Regime in Axion Inflation*, *Phys. Rev. Lett.* **131** (2023) 151003 [[2303.17436](#)].
- [14] A. Caravano, K. Inomata and S. Renaux-Petel, *The Inflationary Butterfly Effect: Non-Perturbative Dynamics From Small-Scale Features*, [2403.12811](#).
- [15] A. A. Starobinsky, *Dynamics of Phase Transition in the New Inflationary Universe Scenario and Generation of Perturbations*, *Phys. Lett. B* **117** (1982) 175.
- [16] A. A. Starobinsky, *STOCHASTIC DE SITTER (INFLATIONARY) STAGE IN THE EARLY UNIVERSE*, *Lect. Notes Phys.* **246** (1986) 107.
- [17] Y. Nambu and M. Sasaki, *Stochastic Stage of an Inflationary Universe Model*, *Phys. Lett. B* **205** (1988) 441.
- [18] Y. Nambu and M. Sasaki, *Stochastic Approach to Chaotic Inflation and the Distribution of Universes*, *Phys. Lett. B* **219** (1989) 240.
- [19] H. E. Kandrup, *STOCHASTIC INFLATION AS A TIME DEPENDENT RANDOM WALK*, *Phys. Rev. D* **39** (1989) 2245.
- [20] K.-i. Nakao, Y. Nambu and M. Sasaki, *Stochastic Dynamics of New Inflation*, *Prog. Theor. Phys.* **80** (1988) 1041.
- [21] Y. Nambu, *Stochastic Dynamics of an Inflationary Model and Initial Distribution of Universes*, *Prog. Theor. Phys.* **81** (1989) 1037.

- [22] S. Mollerach, S. Matarrese, A. Ortolan and F. Lucchin, *Stochastic inflation in a simple two field model*, *Phys. Rev. D* **44** (1991) 1670.
- [23] A. D. Linde, D. A. Linde and A. Mezhlumian, *From the Big Bang theory to the theory of a stationary universe*, *Phys. Rev. D* **49** (1994) 1783 [[gr-qc/9306035](#)].
- [24] A. A. Starobinsky and J. Yokoyama, *Equilibrium state of a selfinteracting scalar field in the De Sitter background*, *Phys. Rev. D* **50** (1994) 6357 [[astro-ph/9407016](#)].
- [25] D. Cruces, *Review on Stochastic Approach to Inflation*, *Universe* **8** (2022) 334 [[2203.13852](#)].
- [26] D. S. Salopek and J. R. Bond, *Stochastic inflation and nonlinear gravity*, *Phys. Rev. D* **43** (1991) 1005.
- [27] T. Fujita, M. Kawasaki, Y. Tada and T. Takesako, *A new algorithm for calculating the curvature perturbations in stochastic inflation*, *JCAP* **12** (2013) 036 [[1308.4754](#)].
- [28] T. Fujita, M. Kawasaki and Y. Tada, *Non-perturbative approach for curvature perturbations in stochastic δN formalism*, *JCAP* **10** (2014) 030 [[1405.2187](#)].
- [29] V. Vennin and A. A. Starobinsky, *Correlation Functions in Stochastic Inflation*, *Eur. Phys. J. C* **75** (2015) 413 [[1506.04732](#)].
- [30] D. G. Figueroa, S. Raatikainen, S. Rasanen and E. Tomberg, *Non-Gaussian Tail of the Curvature Perturbation in Stochastic Ultraslow-Roll Inflation: Implications for Primordial Black Hole Production*, *Phys. Rev. Lett.* **127** (2021) 101302 [[2012.06551](#)].
- [31] D. G. Figueroa, S. Raatikainen, S. Rasanen and E. Tomberg, *Implications of stochastic effects for primordial black hole production in ultra-slow-roll inflation*, *JCAP* **05** (2022) 027 [[2111.07437](#)].
- [32] S. Raatikainen, S. Räsänen and E. Tomberg, *Primordial black hole compaction function from stochastic fluctuations in ultra-slow-roll inflation*, [2312.12911](#).
- [33] V. Atal, J. Cid, A. Escrivà and J. Garriga, *PBH in single field inflation: the effect of shape dispersion and non-Gaussianities*, *JCAP* **05** (2020) 022 [[1908.11357](#)].
- [34] A. Escrivà, C. Germani and R. K. Sheth, *Universal threshold for primordial black hole formation*, *Phys. Rev. D* **101** (2020) 044022 [[1907.13311](#)].
- [35] J. H. P. Jackson, H. Assadullahi, K. Koyama, V. Vennin and D. Wands, *Numerical simulations of stochastic inflation using importance sampling*, *JCAP* **10** (2022) 067 [[2206.11234](#)].
- [36] L. Pinol, S. Renaux-Petel and Y. Tada, *A manifestly covariant theory of multifield stochastic inflation in phase space: solving the discretisation ambiguity in stochastic inflation*, *JCAP* **04** (2021) 048 [[2008.07497](#)].
- [37] C. Pattison, V. Vennin, H. Assadullahi and D. Wands, *Stochastic inflation beyond slow roll*, *JCAP* **07** (2019) 031 [[1905.06300](#)].
- [38] J. Tokuda and T. Tanaka, *Statistical nature of infrared dynamics on de Sitter background*, *JCAP* **02** (2018) 014 [[1708.01734](#)].
- [39] J. Tokuda and T. Tanaka, *Can all the infrared secular growth really be understood as increase of classical statistical variance?*, *JCAP* **11** (2018) 022 [[1806.03262](#)].
- [40] D. Cruces and C. Germani, *Stochastic inflation at all order in slow-roll parameters: Foundations*, *Phys. Rev. D* **105** (2022) 023533 [[2107.12735](#)].
- [41] S. Pi and M. Sasaki, *Logarithmic Duality of the Curvature Perturbation*, *Phys. Rev. Lett.* **131** (2023) 011002 [[2211.13932](#)].
- [42] R. Kawaguchi, T. Fujita and M. Sasaki, *Highly asymmetric probability distribution from a finite-width upward step during inflation*, *JCAP* **11** (2023) 021 [[2305.18140](#)].

- [43] J. H. P. Jackson, H. Assadullahi, A. D. Gow, K. Koyama, V. Vennin and D. Wands, *The separate-universe approach and sudden transitions during inflation*, *JCAP* **05** (2024) 053 [2311.03281].
- [44] T. Fujita, R. Kawaguchi, M. Sasaki and Y. Tada in preparation.
- [45] P. Kloeden and E. Platen, *Numerical Solution of Stochastic Differential Equations*, Stochastic Modelling and Applied Probability. Springer Berlin Heidelberg, 2011.
- [46] L. Pinol, S. Renaux-Petel and Y. Tada, *Inflationary stochastic anomalies*, *Class. Quant. Grav.* **36** (2019) 07LT01 [1806.10126].
- [47] A. A. Starobinsky, *Multicomponent de Sitter (Inflationary) Stages and the Generation of Perturbations*, *JETP Lett.* **42** (1985) 152.
- [48] D. S. Salopek and J. R. Bond, *Nonlinear evolution of long wavelength metric fluctuations in inflationary models*, *Phys. Rev. D* **42** (1990) 3936.
- [49] M. Sasaki and E. D. Stewart, *A General analytic formula for the spectral index of the density perturbations produced during inflation*, *Prog. Theor. Phys.* **95** (1996) 71 [astro-ph/9507001].
- [50] M. Sasaki and T. Tanaka, *Superhorizon scale dynamics of multiscalar inflation*, *Prog. Theor. Phys.* **99** (1998) 763 [gr-qc/9801017].
- [51] D. Wands, K. A. Malik, D. H. Lyth and A. R. Liddle, *A New approach to the evolution of cosmological perturbations on large scales*, *Phys. Rev. D* **62** (2000) 043527 [astro-ph/0003278].
- [52] D. H. Lyth, K. A. Malik and M. Sasaki, *A General proof of the conservation of the curvature perturbation*, *JCAP* **05** (2005) 004 [astro-ph/0411220].
- [53] D. H. Lyth and Y. Rodriguez, *The Inflationary prediction for primordial non-Gaussianity*, *Phys. Rev. Lett.* **95** (2005) 121302 [astro-ph/0504045].
- [54] M. Kawasaki and Y. Tada, *Can massive primordial black holes be produced in mild waterfall hybrid inflation?*, *JCAP* **08** (2016) 041 [1512.03515].
- [55] H. Assadullahi, H. Firouzjahi, M. Noorbala, V. Vennin and D. Wands, *Multiple Fields in Stochastic Inflation*, *JCAP* **06** (2016) 043 [1604.04502].
- [56] V. Vennin, H. Assadullahi, H. Firouzjahi, M. Noorbala and D. Wands, *Critical Number of Fields in Stochastic Inflation*, *Phys. Rev. Lett.* **118** (2017) 031301 [1604.06017].
- [57] C. Pattison, V. Vennin, H. Assadullahi and D. Wands, *Quantum diffusion during inflation and primordial black holes*, *JCAP* **10** (2017) 046 [1707.00537].
- [58] J. M. Ezquiaga and J. García-Bellido, *Quantum diffusion beyond slow-roll: implications for primordial black-hole production*, *JCAP* **08** (2018) 018 [1805.06731].
- [59] M. Noorbala, V. Vennin, H. Assadullahi, H. Firouzjahi and D. Wands, *Tunneling in Stochastic Inflation*, *JCAP* **09** (2018) 032 [1806.09634].
- [60] H. Firouzjahi, A. Nassiri-Rad and M. Noorbala, *Stochastic Ultra Slow Roll Inflation*, *JCAP* **01** (2019) 040 [1811.02175].
- [61] M. Noorbala and H. Firouzjahi, *Boundary crossing in stochastic inflation with a critical number of fields*, *Phys. Rev. D* **100** (2019) 083510 [1907.13149].
- [62] N. Kitajima, Y. Tada and F. Takahashi, *Stochastic inflation with an extremely large number of e-folds*, *Phys. Lett. B* **800** (2020) 135097 [1908.08694].
- [63] T. Prokopec and G. Rigopoulos, *ΔN and the stochastic conveyor belt of ultra slow-roll inflation*, *Phys. Rev. D* **104** (2021) 083505 [1910.08487].
- [64] J. M. Ezquiaga, J. García-Bellido and V. Vennin, *The exponential tail of inflationary fluctuations: consequences for primordial black holes*, *JCAP* **03** (2020) 029 [1912.05399].

- [65] H. Firouzjahi, A. Nassiri-Rad and M. Noorbala, *Stochastic nonattractor inflation*, *Phys. Rev. D* **102** (2020) 123504 [2009.04680].
- [66] A. De and R. Mahbub, *Numerically modeling stochastic inflation in slow-roll and beyond*, *Phys. Rev. D* **102** (2020) 123509 [2010.12685].
- [67] K. Ando and V. Vennin, *Power spectrum in stochastic inflation*, *JCAP* **04** (2021) 057 [2012.02031].
- [68] C. Pattison, V. Vennin, D. Wands and H. Assadullahi, *Ultra-slow-roll inflation with quantum diffusion*, *JCAP* **04** (2021) 080 [2101.05741].
- [69] Y. Tada and V. Vennin, *Statistics of coarse-grained cosmological fields in stochastic inflation*, *JCAP* **02** (2022) 021 [2111.15280].
- [70] J. M. Ezquiaga, J. García-Bellido and V. Vennin, *Massive Galaxy Clusters Like El Gordo Hint at Primordial Quantum Diffusion*, *Phys. Rev. Lett.* **130** (2023) 121003 [2207.06317].
- [71] N. Ahmadi, M. Noorbala, N. Feyzabadi, F. Eghbalpoor and Z. Ahmadi, *Quantum diffusion in sharp transition to non-slow-roll phase*, *JCAP* **08** (2022) 078 [2207.10578].
- [72] A. Nassiri-Rad, K. Asadi and H. Firouzjahi, *Inflation with stochastic boundary*, *Phys. Rev. D* **106** (2022) 123528 [2208.08229].
- [73] C. Animali and V. Vennin, *Primordial black holes from stochastic tunnelling*, *JCAP* **02** (2023) 043 [2210.03812].
- [74] E. Tomberg, *Numerical stochastic inflation constrained by frozen noise*, *JCAP* **04** (2023) 042 [2210.17441].
- [75] A. D. Gow, H. Assadullahi, J. H. P. Jackson, K. Koyama, V. Vennin and D. Wands, *Non-perturbative non-Gaussianity and primordial black holes*, *EPL* **142** (2023) 49001 [2211.08348].
- [76] G. Rigopoulos and A. Wilkins, *Computing first-passage times with the functional renormalisation group*, *JCAP* **04** (2023) 046 [2211.09649].
- [77] V. Briaud and V. Vennin, *Uphill inflation*, *JCAP* **06** (2023) 029 [2301.09336].
- [78] K. Asadi, A. Nassiri-Rad and H. Firouzjahi, *Stochastic multiple fields inflation: Diffusion dominated regime*, *Phys. Rev. D* **108** (2023) 123537 [2304.00577].
- [79] E. Tomberg, *Stochastic constant-roll inflation and primordial black holes*, *Phys. Rev. D* **108** (2023) 043502 [2304.10903].
- [80] Y. Tada and M. Yamada, *Stochastic dynamics of multi-waterfall hybrid inflation and formation of primordial black holes*, *JCAP* **11** (2023) 089 [2306.07324].
- [81] K. Tokeshi and V. Vennin, *Why does inflation look single field to us?*, [2310.16649](#).
- [82] C. Animali and V. Vennin, *Clustering of primordial black holes from quantum diffusion during inflation*, [2402.08642](#).
- [83] E. Komatsu and D. N. Spergel, *Acoustic signatures in the primary microwave background bispectrum*, *Phys. Rev. D* **63** (2001) 063002 [astro-ph/0005036].
- [84] J. M. Maldacena, *Non-Gaussian features of primordial fluctuations in single field inflationary models*, *JHEP* **05** (2003) 013 [astro-ph/0210603].
- [85] F. Vernizzi and D. Wands, *Non-gaussianities in two-field inflation*, *JCAP* **05** (2006) 019 [astro-ph/0603799].
- [86] S. Yokoyama, T. Suyama and T. Tanaka, *Primordial Non-Gaussianity in Multi-Scalar Slow-Roll Inflation*, *JCAP* **07** (2007) 013 [0705.3178].

- [87] S. Yokoyama, T. Suyama and T. Tanaka, *Primordial Non-Gaussianity in Multi-Scalar Inflation*, *Phys. Rev. D* **77** (2008) 083511 [0711.2920].
- [88] Y. Tada and V. Vennin, *Squeezed bispectrum in the δN formalism: local observer effect in field space*, *JCAP* **02** (2017) 021 [1609.08876].
- [89] A. A. Abolhasani and M. Sasaki, *Single-field consistency relation and δN -formalism*, *JCAP* **08** (2018) 025 [1805.11298].
- [90] X. Chen, *Primordial Non-Gaussianities from Inflation Models*, *Adv. Astron.* **2010** (2010) 638979 [1002.1416].
- [91] A. A. Starobinsky, *Spectrum of adiabatic perturbations in the universe when there are singularities in the inflation potential*, *JETP Lett.* **55** (1992) 489.
- [92] S. Pi and J. Wang, *Primordial black hole formation in Starobinsky's linear potential model*, *JCAP* **06** (2023) 018 [2209.14183].
- [93] Y.-F. Cai, X. Chen, M. H. Namjoo, M. Sasaki, D.-G. Wang and Z. Wang, *Revisiting non-Gaussianity from non-attractor inflation models*, *JCAP* **05** (2018) 012 [1712.09998].
- [94] S. Passaglia, W. Hu and H. Motohashi, *Primordial black holes and local non-Gaussianity in canonical inflation*, *Phys. Rev. D* **99** (2019) 043536 [1812.08243].
- [95] S. Hawking, *Gravitationally collapsed objects of very low mass*, *Mon. Not. Roy. Astron. Soc.* **152** (1971) 75.
- [96] B. J. Carr and S. W. Hawking, *Black holes in the early Universe*, *Mon. Not. Roy. Astron. Soc.* **168** (1974) 399.
- [97] B. J. Carr, *The Primordial black hole mass spectrum*, *Astrophys. J.* **201** (1975) 1.
- [98] B. Carr, K. Kohri, Y. Sendouda and J. Yokoyama, *Constraints on primordial black holes*, *Rept. Prog. Phys.* **84** (2021) 116902 [2002.12778].
- [99] A. Escrivà, F. Kuhnel and Y. Tada, *Primordial Black Holes*, **2211.05767**.
- [100] C.-M. Yoo, *The Basics of Primordial Black Hole Formation and Abundance Estimation*, *Galaxies* **10** (2022) 112 [2211.13512].
- [101] B. Carr, S. Clesse, J. Garcia-Bellido, M. Hawkins and F. Kuhnel, *Observational evidence for primordial black holes: A positivist perspective*, *Phys. Rept.* **1054** (2024) 1 [2306.03903].
- [102] P. Amaro-Seoane, H. Audley, S. Babak, J. Baker, E. Barausse, P. Bender et al., *Laser interferometer space antenna*, *arXiv preprint arXiv:1702.00786* (2017) .
- [103] W.-H. Ruan, Z.-K. Guo, R.-G. Cai and Y.-Z. Zhang, *Taiji program: Gravitational-wave sources*, *Int. J. Mod. Phys. A* **35** (2020) 2050075 [1807.09495].
- [104] TIANQIN collaboration, J. Luo et al., *TianQin: a space-borne gravitational wave detector*, *Class. Quant. Grav.* **33** (2016) 035010 [1512.02076].
- [105] S. Kawamura et al., *The Japanese space gravitational wave antenna: DECIGO*, *Class. Quant. Grav.* **28** (2011) 094011.
- [106] B. Carr and J. Silk, *Primordial Black Holes as Generators of Cosmic Structures*, *Mon. Not. Roy. Astron. Soc.* **478** (2018) 3756 [1801.00672].
- [107] H. Niikura, M. Takada, S. Yokoyama, T. Sumi and S. Masaki, *Constraints on Earth-mass primordial black holes from OGLE 5-year microlensing events*, *Phys. Rev. D* **99** (2019) 083503 [1901.07120].
- [108] J. Scholtz and J. Unwin, *What if planet 9 is a primordial black hole?*, *Phys. Rev. Lett.* **125** (2020) 051103.
- [109] E. Witten, *Searching for a Black Hole in the Outer Solar System*, **2004.14192**.

- [110] J. Smirnov, A. Goobar, T. Linden and E. Mörtzell, *White Dwarfs in Dwarf Spheroidal Galaxies: A New Class of Compact-Dark-Matter Detectors*, [2211.00013](#).
- [111] K. S. Phukon, G. Baltus, S. Caudill, S. Clesse, A. Depasse, M. Fays et al., *The hunt for sub-solar primordial black holes in low mass ratio binaries is open*, [2105.11449](#).
- [112] LIGO SCIENTIFIC, VIRGO, KAGRA collaboration, R. Abbott et al., *Search for subsolar-mass black hole binaries in the second part of Advanced LIGO's and Advanced Virgo's third observing run*, *Mon. Not. Roy. Astron. Soc.* **524** (2023) 5984 [[2212.01477](#)].
- [113] M. Prunier, G. Morrás, J. F. N. n. Siles, S. Clesse, J. García-Bellido and E. Ruiz Morales, *Analysis of the subsolar-mass black hole candidate SSM200308 from the second part of the third observing run of Advanced LIGO-Virgo*, [2311.16085](#).
- [114] S. W. Hawking, I. G. Moss and J. M. Stewart, *Bubble Collisions in the Very Early Universe*, *Phys. Rev. D* **26** (1982) 2681.
- [115] H. Kodama, M. Sasaki and K. Sato, *Abundance of Primordial Holes Produced by Cosmological First Order Phase Transition*, *Prog. Theor. Phys.* **68** (1982) 1979.
- [116] I. G. Moss, *Black hole formation from colliding bubbles*, [gr-qc/9405045](#).
- [117] M. Y. Khlopov, R. V. Konoplich, S. G. Rubin and A. S. Sakharov, *Formation of black holes in first order phase transitions*, [hep-ph/9807343](#).
- [118] M. Y. Khlopov, R. V. Konoplich, S. G. Rubin and A. S. Sakharov, *First order phase transitions as a source of black holes in the early universe*, *Grav. Cosmol.* **2** (1999) S1 [[hep-ph/9912422](#)].
- [119] H. Deng and A. Vilenkin, *Primordial black hole formation by vacuum bubbles*, *JCAP* **12** (2017) 044 [[1710.02865](#)].
- [120] A. Kusenko, M. Sasaki, S. Sugiyama, M. Takada, V. Takhistov and E. Vitagliano, *Exploring Primordial Black Holes from the Multiverse with Optical Telescopes*, *Phys. Rev. Lett.* **125** (2020) 181304 [[2001.09160](#)].
- [121] N. Kitajima and F. Takahashi, *Primordial Black Holes from QCD Axion Bubbles*, *JCAP* **11** (2020) 060 [[2006.13137](#)].
- [122] D. N. Maeso, L. Marzola, M. Raidal, V. Vaskonen and H. Veermäe, *Primordial black holes from spectator field bubbles*, *JCAP* **02** (2022) 017 [[2112.01505](#)].
- [123] F. Ferrer, E. Masso, G. Panico, O. Pujolas and F. Rompineve, *Primordial Black Holes from the QCD axion*, *Phys. Rev. Lett.* **122** (2019) 101301 [[1807.01707](#)].
- [124] G. B. Gelmini, A. Simpson and E. Vitagliano, *Catastrogenesis: DM, GWs, and PBHs from ALP string-wall networks*, *JCAP* **02** (2023) 031 [[2207.07126](#)].
- [125] G. B. Gelmini, J. Hyman, A. Simpson and E. Vitagliano, *Primordial black hole dark matter from catastrogenesis with unstable pseudo-Goldstone bosons*, *JCAP* **06** (2023) 055 [[2303.14107](#)].
- [126] Y. Gouttenoire and E. Vitagliano, *Primordial Black Holes and Wormholes from Domain Wall Networks*, [2311.07670](#).
- [127] D. I. Dunskey and M. Kongsore, *Primordial Black Holes from Axion Domain Wall Collapse*, [2402.03426](#).
- [128] S. Passaglia and M. Sasaki, *Primordial black holes from CDM isocurvature perturbations*, *Phys. Rev. D* **105** (2022) 103530 [[2109.12824](#)].
- [129] C.-M. Yoo, T. Harada, S. Hirano, H. Okawa and M. Sasaki, *Primordial black hole formation from massless scalar isocurvature*, *Phys. Rev. D* **105** (2022) 103538 [[2112.12335](#)].

- [130] G. Dvali, F. Kühnel and M. Zantedeschi, *Primordial black holes from confinement*, *Phys. Rev. D* **104** (2021) 123507 [2108.09471].
- [131] Y. Tada and S. Yokoyama, *Primordial black hole tower: Dark matter, earth-mass, and LIGO black holes*, *Phys. Rev. D* **100** (2019) 023537 [1904.10298].
- [132] M. Shibata and M. Sasaki, *Black hole formation in the friedmann universe: Formulation and computation in numerical relativity*, *Phys. Rev. D* **60** (1999) 084002.
- [133] T. Harada, C.-M. Yoo, T. Nakama and Y. Koga, *Cosmological long-wavelength solutions and primordial black hole formation*, *Phys. Rev. D* **91** (2015) 084057.
- [134] M. W. Choptuik, *Universality and scaling in gravitational collapse of a massless scalar field*, *Phys. Rev. Lett.* **70** (1993) 9.
- [135] C. R. Evans and J. S. Coleman, *Observation of critical phenomena and selfsimilarity in the gravitational collapse of radiation fluid*, *Phys. Rev. Lett.* **72** (1994) 1782 [gr-qc/9402041].
- [136] T. Koike, T. Hara and S. Adachi, *Critical behavior in gravitational collapse of radiation fluid: A Renormalization group (linear perturbation) analysis*, *Phys. Rev. Lett.* **74** (1995) 5170 [gr-qc/9503007].
- [137] J. C. Niemeyer and K. Jedamzik, *Near-critical gravitational collapse and the initial mass function of primordial black holes*, *Phys. Rev. Lett.* **80** (1998) 5481 [astro-ph/9709072].
- [138] J. C. Niemeyer and K. Jedamzik, *Dynamics of primordial black hole formation*, *Phys. Rev. D* **59** (1999) 124013 [astro-ph/9901292].
- [139] I. Hawke and J. M. Stewart, *The dynamics of primordial black hole formation*, *Class. Quant. Grav.* **19** (2002) 3687.
- [140] I. Musco, J. C. Miller and A. G. Polnarev, *Primordial black hole formation in the radiative era: Investigation of the critical nature of the collapse*, *Class. Quant. Grav.* **26** (2009) 235001 [0811.1452].
- [141] J. M. Bardeen, J. R. Bond, N. Kaiser and A. S. Szalay, *The Statistics of Peaks of Gaussian Random Fields*, *Astrophys. J.* **304** (1986) 15.
- [142] C.-M. Yoo, T. Harada, J. Garriga and K. Kohri, *Primordial black hole abundance from random Gaussian curvature perturbations and a local density threshold*, *PTEP* **2018** (2018) 123E01 [1805.03946].
- [143] C.-M. Yoo, J.-O. Gong and S. Yokoyama, *Abundance of primordial black holes with local non-Gaussianity in peak theory*, *JCAP* **09** (2019) 033 [1906.06790].
- [144] C.-M. Yoo, T. Harada, S. Hirano and K. Kohri, *Abundance of Primordial Black Holes in Peak Theory for an Arbitrary Power Spectrum*, *PTEP* **2021** (2021) 013E02 [2008.02425].
- [145] N. Kitajima, Y. Tada, S. Yokoyama and C.-M. Yoo, *Primordial black holes in peak theory with a non-Gaussian tail*, *JCAP* **10** (2021) 053 [2109.00791].
- [146] C. Germani and R. K. Sheth, *Nonlinear statistics of primordial black holes from Gaussian curvature perturbations*, *Phys. Rev. D* **101** (2020) 063520 [1912.07072].
- [147] C. Germani and R. K. Sheth, *The Statistics of Primordial Black Holes in a Radiation-Dominated Universe: Recent and New Results*, *Universe* **9** (2023) 421 [2308.02971].
- [148] PLANCK collaboration, N. Aghanim et al., *Planck 2018 results. VI. Cosmological parameters*, *Astron. Astrophys.* **641** (2020) A6 [1807.06209].
- [149] C.-M. Yoo, T. Harada and H. Okawa, *Threshold of Primordial Black Hole Formation in Nonspherical Collapse*, *Phys. Rev. D* **102** (2020) 043526 [2004.01042].
- [150] Y. Tada and M. Yamada, *Multifield Stochastic Dynamics in GUT Hybrid Inflation and Gravitational Wave Signatures of GUT Higgs Representation*, 2405.08859.

- [151] D. H. Lyth, *Contribution of the hybrid inflation waterfall to the primordial curvature perturbation*, *JCAP* **07** (2011) 035 [[1012.4617](#)].
- [152] D. H. Lyth, *The hybrid inflation waterfall and the primordial curvature perturbation*, *JCAP* **05** (2012) 022 [[1201.4312](#)].
- [153] E. Bugaev and P. Klimai, *Curvature perturbation spectra from waterfall transition, black hole constraints and non-Gaussianity*, *JCAP* **11** (2011) 028 [[1107.3754](#)].
- [154] E. Bugaev and P. Klimai, *Formation of primordial black holes from non-Gaussian perturbations produced in a waterfall transition*, *Phys. Rev. D* **85** (2012) 103504 [[1112.5601](#)].
- [155] P. Auclair and C. Ringeval, *Slow-roll inflation at N3LO*, *Phys. Rev. D* **106** (2022) 063512 [[2205.12608](#)].